J. S. Afr. Inst. Min. Metall., vol. 87, no. 6.
Jun. 1987. pp. 163-188.

A fractographic study of corrosion-fatigued specimens of A533B steel

by J.H. BULLOCH*

SYNOPSIS

This paper describes detailed fractographic analyses of several specimens that had undergone corrosion-fatigue tests at high stress ratios in simulated pressurized water-reactor environments.

The distribution and morphology of non-metallic manganese sulphide inclusions are shown to strongly affect the growth of environmentally assisted cracks (EAC), and certain features suggest that a hydrogen-assisted mechanism is responsible for the observed EAC growth. The incidence of transient EAC growth in isolated regions suggests that the critical conditions that trigger this type of growth are the 'right' local chemistry at the crack tips and imposed mechanical conditions.

SAMEVATTING

Hierdie referaat beskryf uitvoerige fraktografiese ontledings van verskeie toetsstukke wat by hoë spannings-verhoudings in gesimuleerde water afkomstig van 'n drukwaterreaktor aan korrosievermoeidheidstoetse onderwerp is.

Daar word getoon dat die verdeling en morfologie van nie-metaalmangaansulfiedinsluitsels 'n sterk uitwerking op die groei van omgewinggesteunde krake (OSK) het en sekere aspekte dui daarop dat 'n waterstofgesteunde meganisme vir die waargenome groei van OSK verantwoordelik is. Die voorkoms van kortstondige groei van OSK in geïsoleerde streke dui daarop dat die kritieke toestande wat tot hierdie tipe groei aanleiding gee, die 'regte' plaaslike chemie by die punt van die kraak en opgelegde meganiese toestande is.

INTRODUCTION

In 1982, an assessment was made of the available data on the growth of environmentally assisted cracks (EAC) —resulting from corrosion fatigue and stress–corrosion cracking—in reactor pressure vessel (RPV) steels in a pressurized water reactor (PWR) environment[1]. It was found that the data were somewhat limited inasmuch that they did not cover the range of parameters—mechanical (stress ratio, frequency), material, and electrochemical—that a reactor in the United Kingdom is likely to experience, they did not provide a sound basis for the extrapolation of data, and a mechanistic rationale of EAC growth was still awaiting clarification.

As a result of these limitations, an experimental collaborative programme was initiated to investigate the above shortcomings. The first phase of this programme, that involving tests at high stress ratios has been completed[2]; this was essentially an attempt to generate and compare the data on fatigue-crack growth with those of Bamford[3], upon which the ASME XI (1980) high stress ratio 'wet' design line is based.

The present report describes fractographic analyses in a number of fatigue tests from the above programme, and in a test from the waveform programme of Babcock Power Ltd (BPL)—Table I. Special emphasis is placed on the role of non-metallic inclusions (essentially manganese sulphides) in EAC behaviour.

TABLE I
DETAILS OF THE TEST SPECIMENS

Laboratory	Test	Waveform	Steel origin	%, S	Orientation
BPL	A1	Sine	M/Frere	0,006	L-S
BPL	A2	Sine	M/Frere	0,006	L-S
BPL	A3	Triangle	M/Frere	0,006	L-S
CERL	A4	Sine	M/Frere	0,006	L-S
BPL	C1*	Sine	M/Frere	0,006	L-S
BPL	C*2	Sine	M/Frere	0,006	L-S
RR & A	C*3	Sine	BSC	0,012	T-L

DETAILS OF FATIGUE-CRACK GROWTH

The growth of fatigue cracks in the various tests listed in Table I is shown in Figs. 1 and 2. These diagrams show that, although the trends in the rates of crack growth are variable, the behaviour can be described by four discrete regions with increasing stress intensity, ΔK. These are shown schematically in Fig. 3 and are defined as follows.

(a) *Region I (air-crack region)* occurs at initial ΔK test levels during which the growth rates lie on the ASME (American Society of Mechanical Engineers) air line and no EAC growth is observed.

(b) *Region II (threshold-crack region)* has a dramatically increased growth rate over a very small range of ΔK (1 to 2 MPa $\sqrt{m}$) and represents the onset or threshold for EAC growth.

(c) *Region III (plateau-crack region)* has constant rates of crack growth, which are independent of the ΔK level. The start of this region represents the maximum extent of EAC growth. The region can span a ΔK

* Senior Research Officer, Department of Metallurgy, University of the Witwatersrand, 1 Jan Smuts Avenue, Johannesburg 2001.

ISSN 0038-223X/$3.00 + 0.00. Paper received 3rd April, 1986.

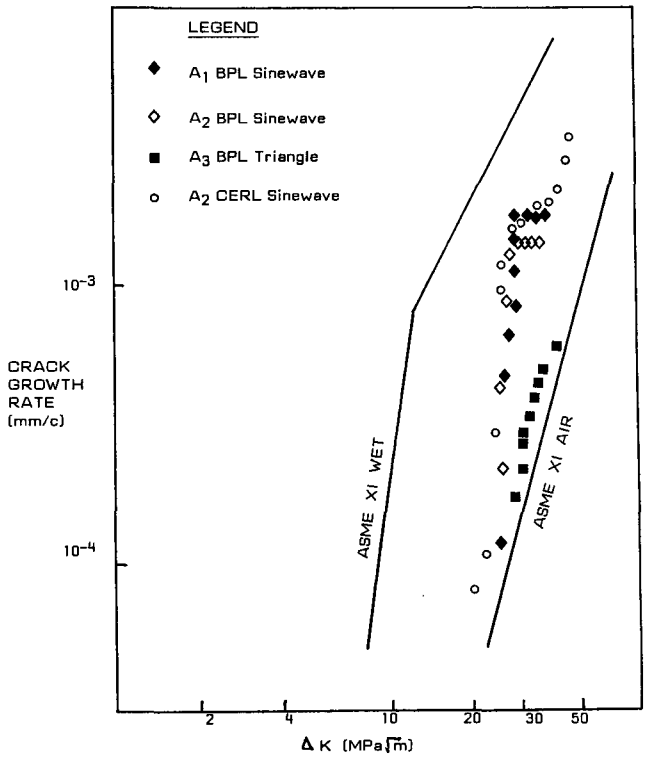

Fig. 1—Fatigue-crack growth in Marrel-Frere A533B steel in a PWR environment under test conditions—R = 0,7, ν = 1 cycle per minute

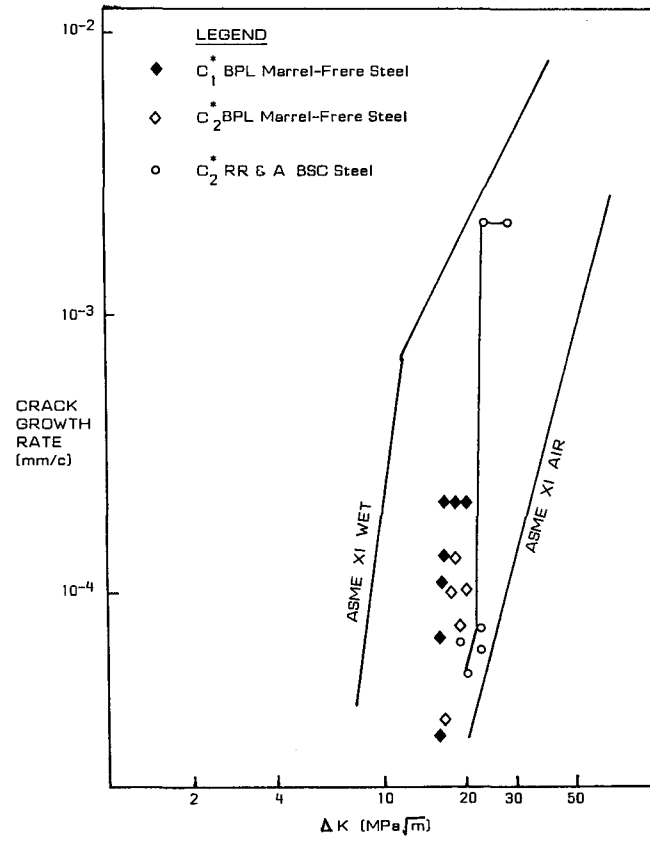

Fig. 2—Fatigue-crack growth in A533B steel in a PWR environment under test C* conditions—R = 0,85, ν = 1 cycle per minute

range from 2 to 15 MPa $\sqrt{m}$, depending on the onset or occurrence of region IV.

(d) *Region IV (post-plateau air-crack region)* has growth rates that lie near the ASME air line, and little EAC growth is observed.

FRACTOGRAPHIC DETAILS

The general fractographic observations in the present study are listed and defined as follows.

(1) *Ductile striated growth.* The general features of this fracture mode are (a) evidence of secondary cracking, (b) the rather amorphous fracture surface, which shows no evidence of river pattern lines parallel to the direction of crack growth, (c) the occurrence of a large number of deep fissures at right angles to the direction of growth, and (d) the patchy occurrence of fine striations, the spacing of which in some cases agrees well with the recorded rate of crack growth. Such a fracture mode occurs predominantly in crack-growth regions I and IV, and to some extent in region III.

(2) *Fan-shaped growth.* The general features of this fracture mode are (a) the many discrete fans on the fatigue surface, which show cleavage-like river pattern lines that run parallel to the direction of crack growth, (b) no evidence of deep fissure formations, (c) a fracture surface that is not flat or amorphous, and (d) fine striation-like details that can sometimes be observed running across the fan-shaped details. This fracture mode occurs predominantly in crack-growth regions II and III.

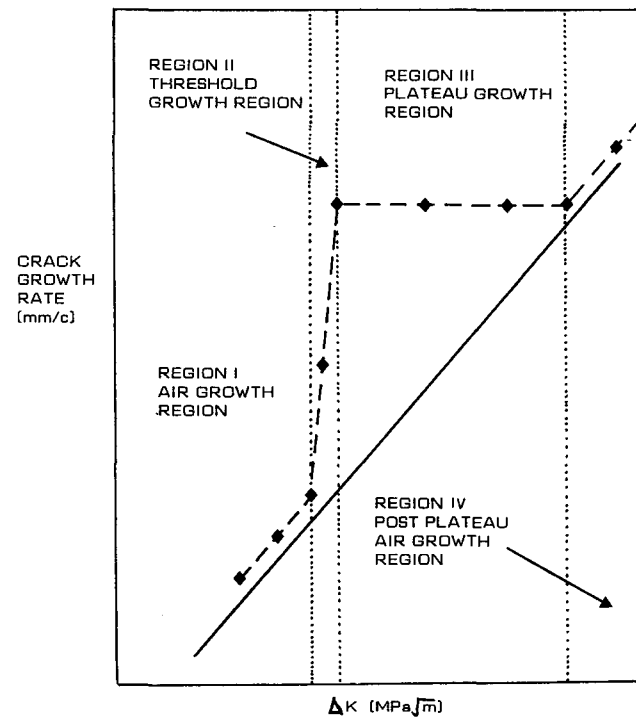

Fig. 3—Schematic details of the various regions of fatigue-crack growth observed in a PWR environment

(3) *Rosette formation.* This is the occurrence of a large (several millimetres) semi-circular formation consisting of micro fan-shaped crack growth that is surrounded by ductile striated growth. It has a distinct initiation site and grows out from this point in an arc of 180 degrees in the general direction of crack growth.

(4) *Pre-threshold EAC growth.* The extent of this growth can vary from small isolated areas to areas of several millimetres. It is similar to rosette formation but does not have the directionality. Both (3) and (4) are instances of the occurrence of isolated patches of region II crack growth in otherwise predominantly region I crack growth.

(5) *Inclusions of manganese sulphide.* Generally, two types of manganese sulphide inclusions were encountered in the present investigation: type I (spherical) inclusions, and type II (rod-like) inclusions. The type I inclusions tended to be evenly distributed throughout the steel matrix, though occasional segregated regions were observed. The type II inclusions were invariably encountered in segregated clusters that sometimes measured several millimetres. Only the vacant sites at which the manganese sulphide inclusions had resided were evident in this particular study, since such inclusions dissolve in a PWR environment.

TEST DETAILS

The details of the water chemistry in various tests are given in Table II, and a general summary of the crack-growth regions observed in the various test specimens is given in Table III. All the tests were high-R tests (R = minimum load/maximum load), and the cyclic frequency, ν, was one cycle per minute.

TABLE II
DETAILS OF THE WATER CHEMISTRY IN THE TESTS

Test source	Dissolved oxygen p.p.b.	Additions of boric acid	Chloride p.p.b.	Sulphate p.p.b.
BPL	<10	Yes	100	1000 to 3000
CERL	<10	Yes*	100	<100
RR & A	<10	Yes	100	1000 to 3000

*Additions of analar boric acid

TABLE III
CRACK GROWTH BEHAVIOUR

Test	Region I	Region II	Region III	Region IV
A1	Yes	Yes	Yes	No
A2	No	Yes	Yes	No
A3	Yes	No	No	No
A4	Yes	Yes	Yes	Yes
C*1	No	Yes	Yes†	No
C*2	Yes	Partially‡	No	No
C*3	Yes	Yes	Yes	No

† Growth in plateau region III was in the ductile striated mode
‡ Macro rosette formation

RESULTS OF SERIES A TESTS

In this series of tests, R was equal to 0,7.

Test A1 (Sinewave)

In the initial growth stages (region I), $\Delta K \approx 26$ MPa $\sqrt{m}$ ($da/dN = 2 \times 10^{-4}$ mm per cycle), the surface of the fatigue fracture was covered predominantly with ductile striations (Fig. 4). Little evidence of inclusion sites was evident. At about 1 mm from the pre-cracked area, $\Delta K = 27$ MPa $\sqrt{m}$, many sites or holes associated with inclusions and/or inclusion clusters were observed. These varied in size up to a maximum length of about 0,2 mm, and were oriented perpendicular to the direction of crack growth, as shown in Fig. 5(a). A magnified view of one of these elongated sites is given in Fig. 5(b), showing that the general fracture mode is still ductile striations. Such sites probably arise from a cluster or grouping of manganese sulphide stringers that dissolved during testing. At the ΔK level immediately before plateau formation (region II), viz 28 to 30 MPa $\sqrt{m}$, the preponderance of these large elongated prior inclusion sites increased—Fig. 6(a). An interesting feature was the association of fan-shaped growth associated with these sites, as shown in Fig. 6(b). A detailed view of these fan-shaped areas, Fig. 6(c), showed that striated growth occurred in some instances, but in others it was not observed. The measured spacing of the striations within the crack growth was about 1,8 to 4,0 $\times 10^{-3}$ mm, which shows some agreement with the recorded macro growth rates.

At ΔK levels beyond the plateau formation (region IV), the general fractographic features did not change greatly, viz there were still many instances of elongated inclusion sites and the fracture mode was predominantly fan-shaped in nature.

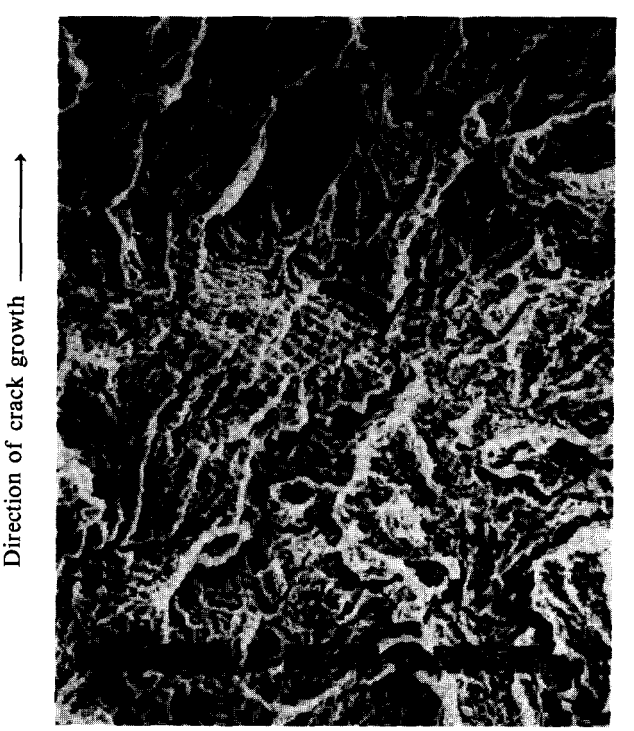

Fig. 4—Just beyond the start of crack growth, ΔK = 26,3 MPa $\sqrt{m}$. Fully ductile striated growth in which there was little evidence of non-metallic inclusions

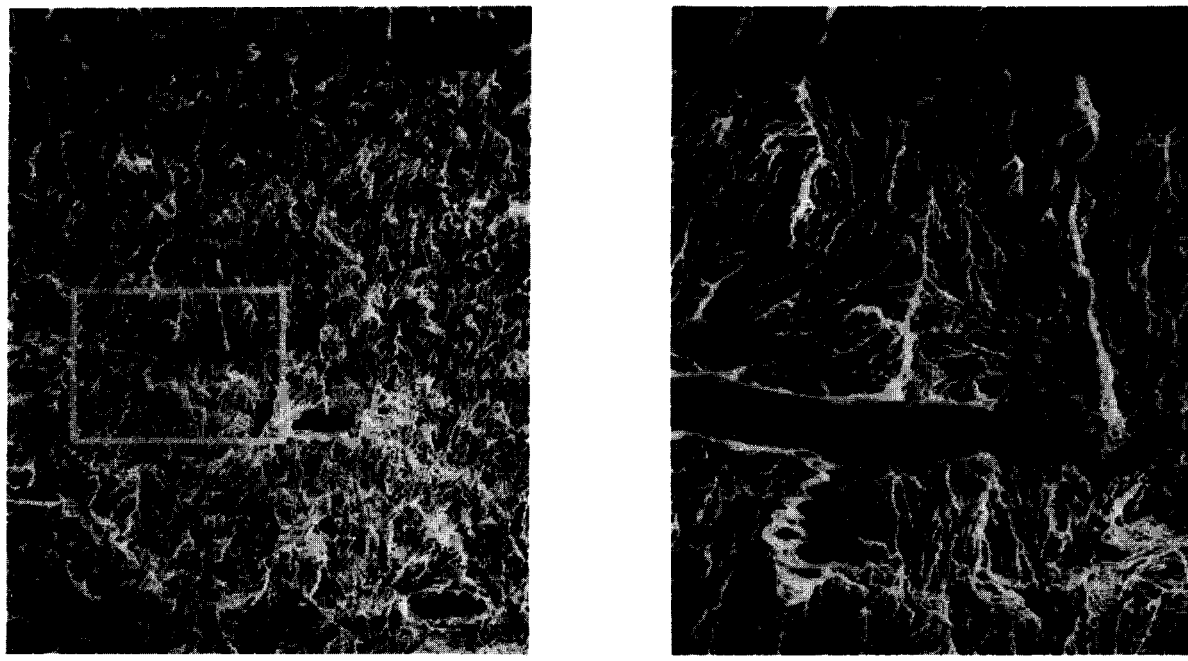

(a) (b)

Fig. 5—ΔK = 27,1 MPa $\sqrt{m}$. The incidence of many long inclusion sites perpendicular to the direction of crack growth, the fracture mode being predominantly that of ductile striations

Generally, the main fracture mode throughout the ΔK range tests was fan-shaped growth showing evidence of striations. Features of note were (a) the large incidence of elongated inclusion sites, about 0,2 mm maximum, perpendicular to the growth direction at ΔK levels around the plateau (region III), and (b) fan-shaped facets, which grew out in the growth direction from these inclusion sites, i.e. not always exhibiting striated growth.

Test A2 (Sinewave)

At the imposed ΔK level of 26 MPa $\sqrt{m}$, region II crack growth occurred immediately, and a significant change in fracture morphology between this EAC region and the air-precracked region was evident (Fig. 7). The precracked region exhibited a flat topology and fissures running perpendicular to the direction of crack growth; this is typical of transgranular ductile striated growth. Region II was covered with a fan-shaped type of growth, with little evidence of fissuring. A general view of the fan-shaped fracture surface is shown in Fig. 8(a). A detailed view showed some fan-shaped areas that did not exhibit much striated growth, Fig. 8(b), while other areas did, Fig. 8(c). The average spacing of the striations in such areas was $1,3 \times 10^{-3}$ mm, which agrees well with the recorded determinations of growth rate.

A general feature was the high incidence of elongated non-metallic inclusion sites at right angles to the direction of growth. An interesting feature, Fig. 9(a) and (b), was the existence of fan-shaped regions, showing little evidence of striated growth, that projected out from the inclusion edges while immediately in front of these inclusion sites striated growth was clearly evident.

Many instances of large elongated clusters of inclusions exceeding 1 mm in length were observed (Fig. 10), and individual inclusion sites within each cluster were clearly evident.

Generally, the total fracture surface was covered in fan-shaped facets that either did or did not exhibit striated growth.

Test A4 (Triangle Wave)

A general view of the initial 4 mm of growth in the triangle waveform is shown in Fig. 11. Again, as in the sinusoidal waveform test, there was a high incidence of elongated inclusion clusters, 0,1 to 0,4 mm long, running perpendicular to the direction of crack growth. Fractographic study established that, at all ΔK levels, the predominant fracture mode was one of transgranular ductile striated growth (region I) characterized by flat topography with fissures at right-angles to the direction of growth (Fig. 12). Around the vast majority of these clusters, no fan-shaped type growth was observed and the fracture mode was predominantly ductile striated growth. However, at two isolated areas on the fracture surface, fan-shaped growth was observed, as illustrated in Figs. 13(a) and (b). These isolated areas were about 1 to 1,5 mm long and started at the elongated sites of non-metallic inclusions. The nature of the fan-shaped growth is shown in Fig. 13(c) and is similar to that widely observed in the sine waveform test.

Test A4 (Sinewave)

A section (Fig. 14) of the broken fracture surface from CERL test A2 was supplied to BPL for fractographic analysis.

Pre-threshold—Region I

The dark band near the middle of the section in Fig. 14 is the region of fatigue-crack growth that occurred at ΔK levels below the 'threshold' ΔK value of about 25 MPa $\sqrt{m}$. An interesting macro-feature within this dark band is the occurrence of elongated light patches across

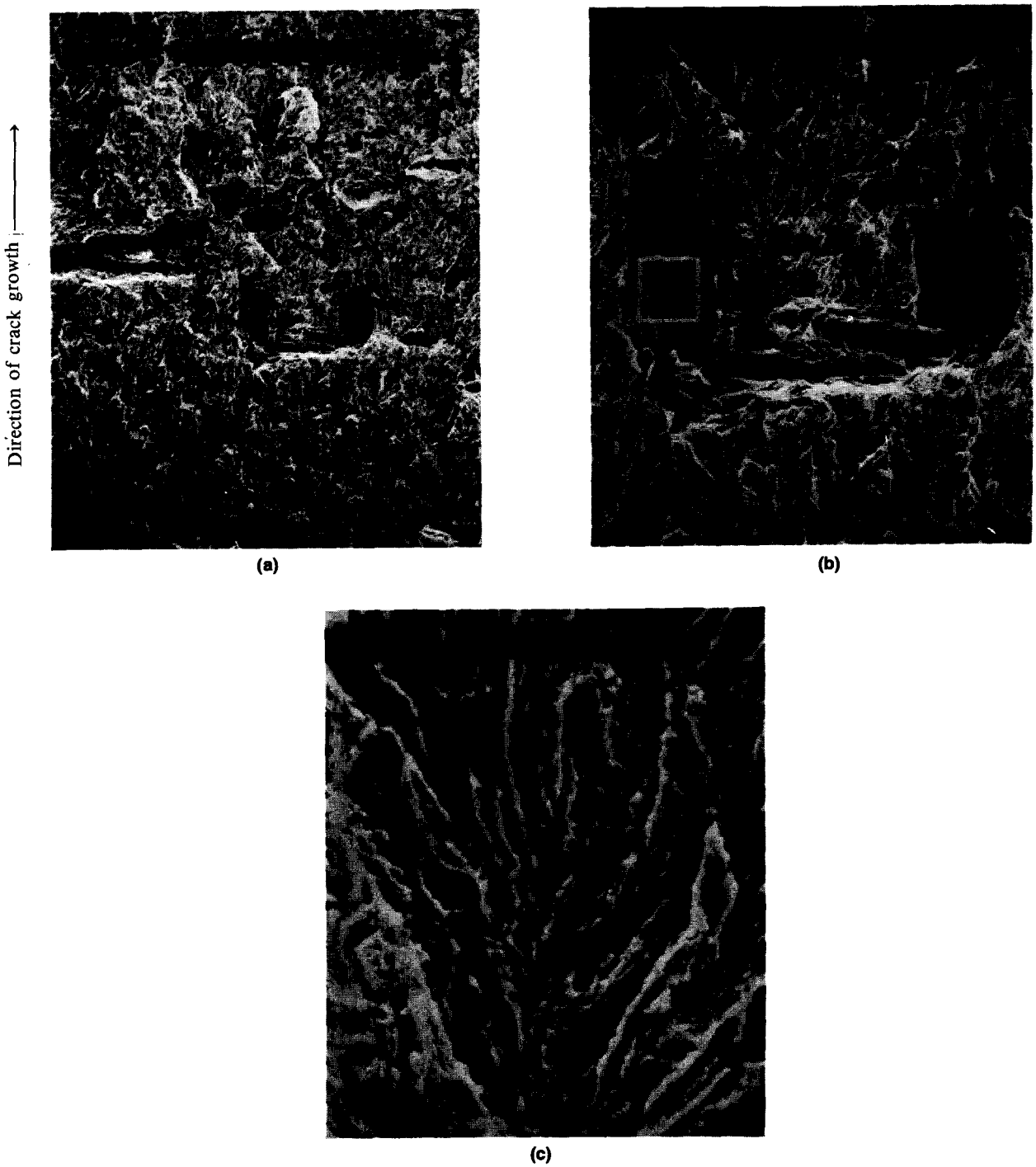

Fig. 6—ΔK region immediately before plateau formation
(a) Many incidences of stringer-like inclusion sites
(b) Fan-shaped region emanating from fan-shaped facets
(c) Detail of fan-shaped faceted region

the width of the test specimen. These light patches were not unlike the light area beyond the region I air-crack growth, i.e. they showed the growth of environmentally assisted fatigue cracks. The markings surrounding these light patches were scribed onto the fracture face for easy identification, and an example is shown in Fig. 15(a). Immediately in front of this light patch are incidences of the elongated inclusion sites that are shown in Fig. 15(b). The difference between the general fractographic nature of the light patch and the darker crack growth is evident in Figs. 16(a) and (b) respectively. The fracture mode in the light patch appears generally fan-shaped, while the other growth region exhibits a rather amorphous appearance with fissures perpendicular to the general direction of crack growth; the latter is typical of ductile striated growth. The border region between the light patch and the darker growth region is shown in Fig. 16(c), which shows the abrupt transition from an amorphous type of surface with fissures to a fan-shaped type showing little evidence of fissures.

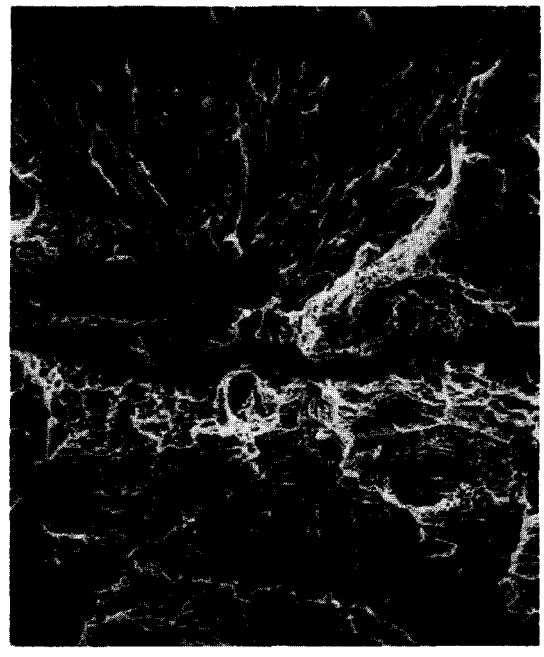

Fig. 7—Boundary between EAC growth (top) and air-precracked region (bottom). The EAC growth region exhibits a fan-shaped faceted type of growth, whereas the air-precracked region shows a much flatter topography, with fissures at right-angles to the direction of growth. The latter is typical of the growth of ductile striated fatigue cracks

These fractographs give clear evidence that the light patches have quite different fractographic features from those of the air-crack growth, i.e. region I.

Crack Growth Beyond Region I

The general impression of the initial stages of growth was one of a high incidence of elongated holes (about 0,3 mm) running perpendicular to the direction of crack growth. These holes result from non-metallic clusters or stringers, and are shown in Fig. 17. Fig. 17(a) shows the general incidence of inclusion sites, while Fig. 17(b) shows typical fan-shaped areas associated with such sites, together with evidence of inclusion cluster sites within those holes.

The fan-shaped areas in some instances exhibited striated growth, Figure 18(a), while less striated growth was observed in others, Fig. 18(b). The average spacing in striated areas was $1{,}8 \times 10^{-3}$ mm, which is of the order of the macro fatigue-crack growth rate at these ΔK levels.

At plateau ΔK levels (region III), flat, rather featureless regions associated with inclusion sites became common, the details being shown in Fig. 19. The general nature of these regions is shown in Fig. 19(a). Within these flat regions, about 0,3 mm in size, striated growth is predominant. A detailed view of these flat areas is given in Fig. 19(b).

The elongated light patches present in the air-crack growth region I of the CERL Test A2 yielded some interesting features. The fracture surface in this area was amorphous, with many fissures perpendicular to the crack growth, which is typical of a ductile striated fracture mode. However, the surface of the light patches consisted almost totally of fan-shaped facets with no evidence of fissuring. Indeed, the fractography of the light patches and the oxide covering were very similar to those of the fast-growth post-threshold area, suggesting that these light patches represent instances of isolated fast-growth regions within the general type of crack growth in region I.

RESULTS OF SERIES C* TESTS

In this series of tests, R was equal to 0,85.

Test C*1 (Sinewave)

The initial stages of growth comprised a fan-shaped growth issuing from the precracked region. Along the width of the specimen, this region of fan-shaped growth varied between 0,3 and 0,5 mm. In several instances, this type of crack growth took the form of parallel rows of fans issuing from specific initiation sites, and are illustrated in Fig. 20. Each discrete fan was about 0,6 mm in width and about 0,4 mm in length. Immediately preceding the region of fan-shaped cracks is a large preponderance of elongated 'holes'. Upon closer inspection, Figs. 21(a) and (b), these 'holes' were identified as clusters of elongated non-metallic inclusions 0,02 mm in diameter that had dissolved during environmental testing. Also, such regions coincided with the initiation point of many individual fan-shaped facets. Fig. 22 shows details of the regions of fan-shaped growth. Without this initial 0,3 to 0,5 mm of fan-shaped growth, the fracture surface was rather flat, with many fissures developing at right angles to the general direction of crack growth; such features are typical of transgranular ductile striated growth. Details of this fracture mode are shown in Fig. 23.

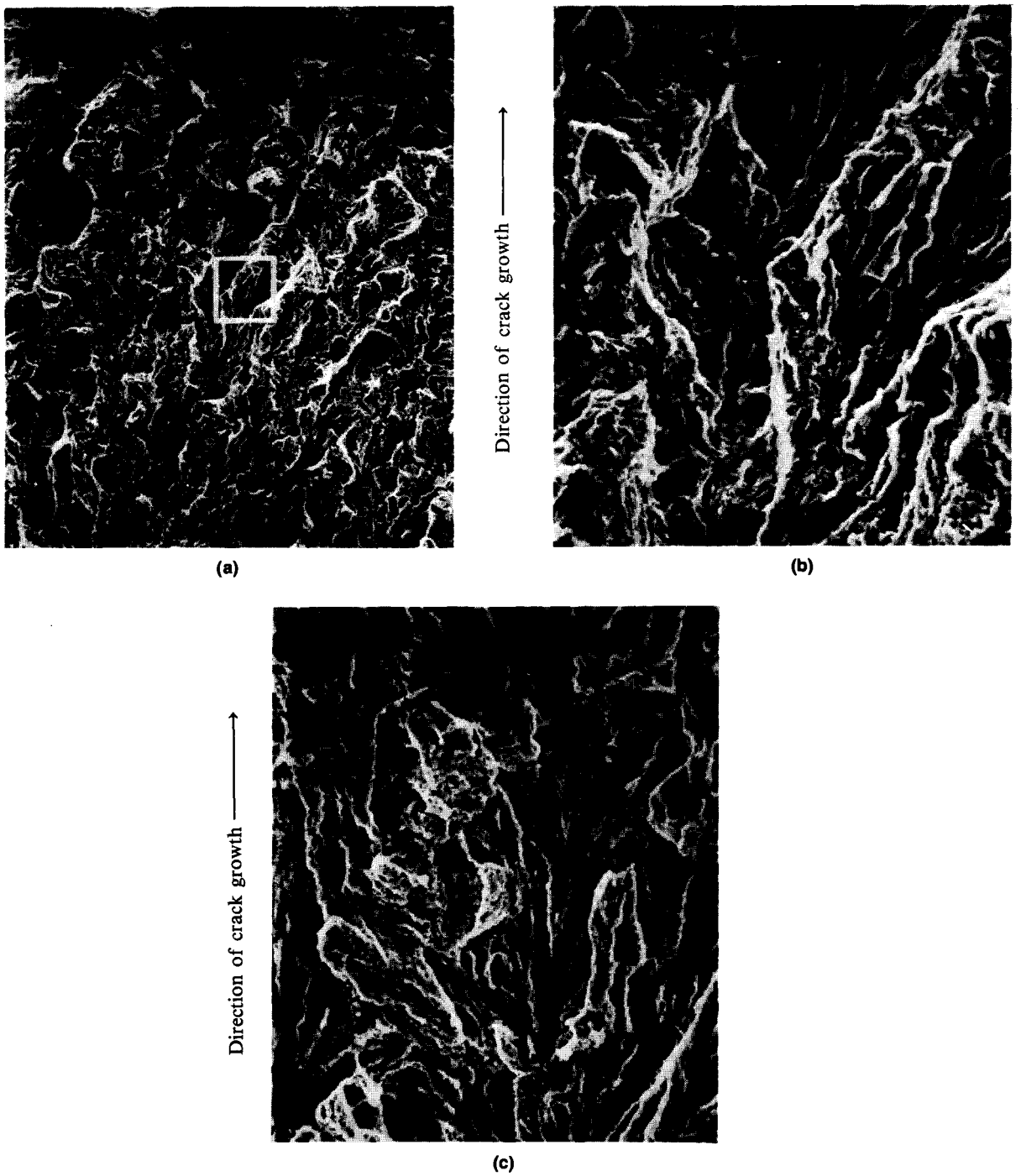

Fig. 8—General fracture surface, showing a preponderance of fan-shaped growth. Striated growth is absent in some of these areas (a) and occurs in others (c)

Test C*2 (Sinewave)

On visual inspection of the broken half-specimen, a macro rosette was observed that was much lighter in colour than the surrounding increment of fatigue-crack growth—about 8 mm wide and 1,7 mm long in the direction of crack growth. Macrographs illustrating this rosette on an oxidized broken half of the specimen are shown in Figs. 24(a) and (b). It is evident that this rosette occurred at a distance of 0,7 mm from the precracked boundary.

On the oxide-stripped fracture surface, the nature of this rosette was examined under the scanning electron microscope (SEM), and a composite picture of the region is shown in Fig. 25. The light rosette of Fig. 24 is shown between the two volcano-type features (initiation sites) and the broken line; the post-test fracture region is evident at the bottom of Fig. 25. Along the boundary of the rosette (broken lines), the morphology of the fracture surface changes fairly abruptly (Fig. 26) inasmuch

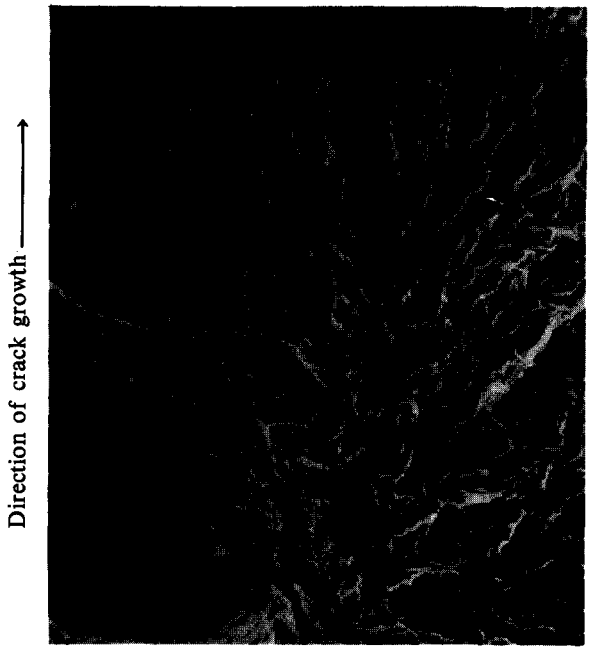

Fig. 9—Incidences of fan-shaped growth running out from the edge of an inclusion. Striated growth occurs in the area immediately before the inclusion. In the area of fan-shaped crack growth running out from the inclusion edge, no such striated growth is evident

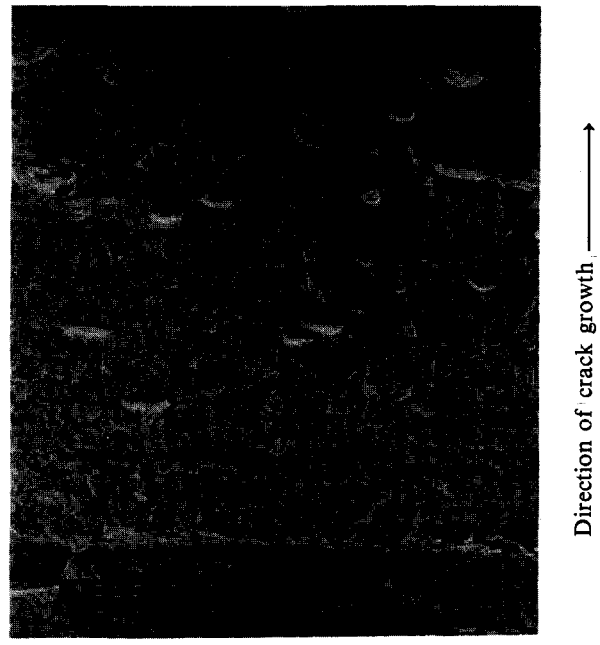

Fig. 11—General view showing the high incidence of inclusion clusters running perpendicular to the direction of crack growth

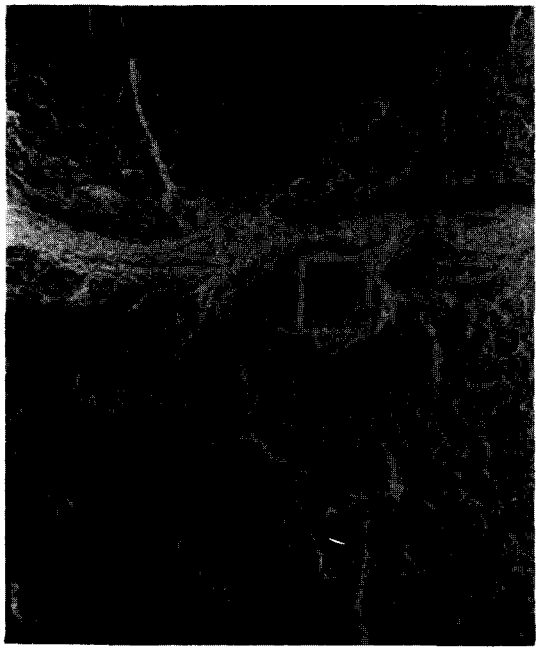

Fig. 10—Incidence of a large inclusion cluster about 1,3 mm long at right-angles to the direction of crack growth. Individual inclusion sites are apparent (white boxed area)

Fig. 12—There is little evidence of fan-shaped growth around the inclusion site. The fracture surface is typically one of ductile striated fatigue-crack growth

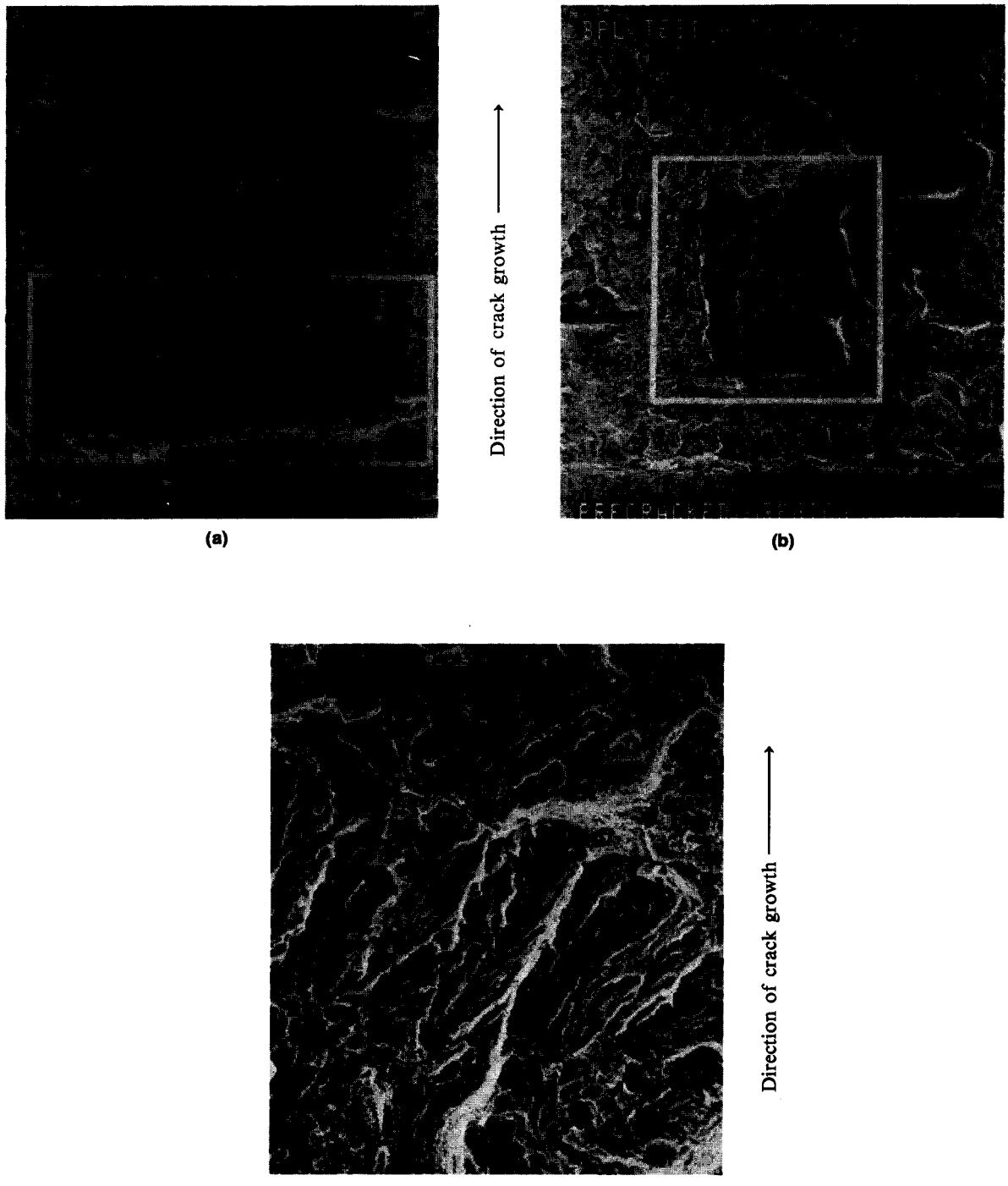

Fig. 13—Two isolated instances, (a) and (b), of areas showing fan-shaped growth that starts at or around clusters of inclusions. Details of the fan-shaped area are shown in (c)

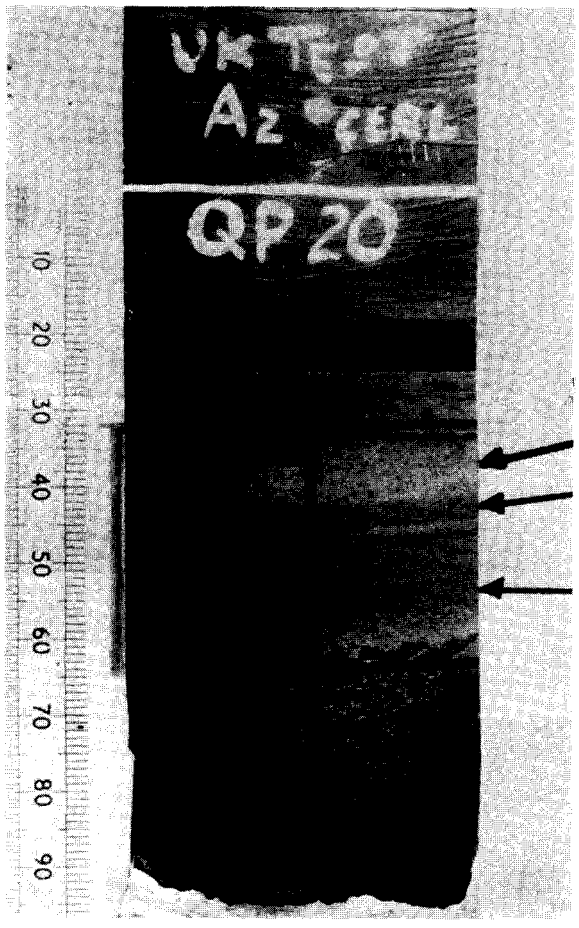

Air pre-cracking region

Pre-threshold ΔK slow-growth region

Post-threshold ΔK fast environmentally assisted growth region

Fig. 14—Broken half of specimen from test A4, showing the section supplied to Babcock Power Limited (× 1,08)

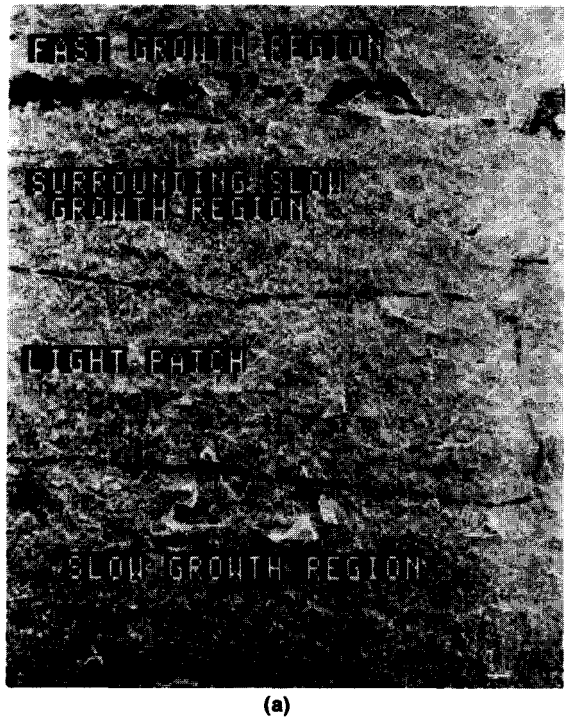

(a)

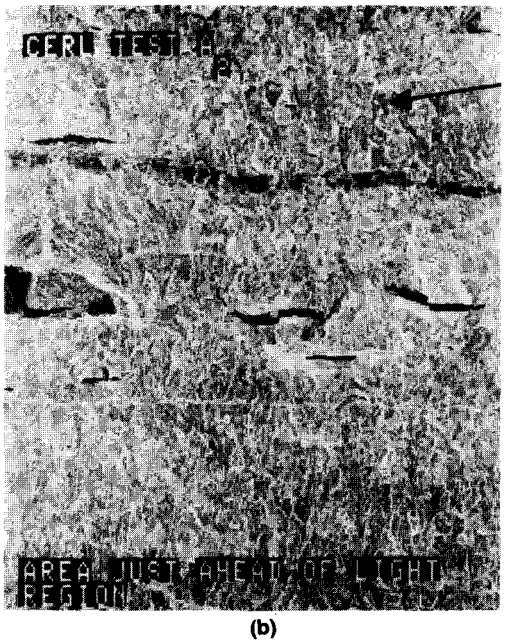

Light patch

(b)

Fig. 15—Characteristics of a light patch surrounded by a region of slow crack growth
(a) The various regions on the surface of the fracture in CERL test A
(b) Elongated inclusion sites immediately in front of the light patch

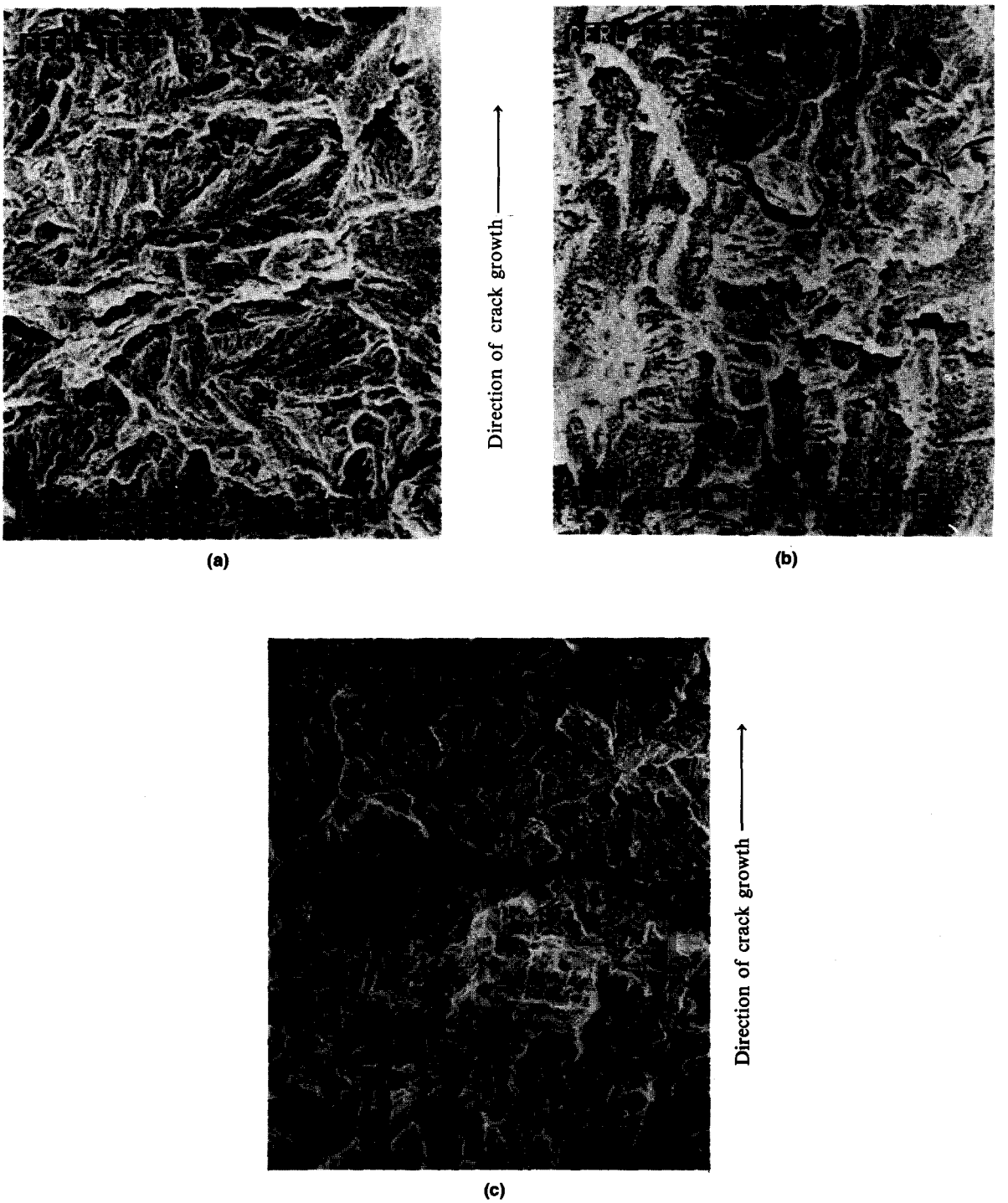

Fig. 16—Characteristics of the light patch surrounded by the region of slow crack growth (Fig. 15)
(a) General fan-shaped nature of the cracks within the light patch
(b) General amorphous nature of the cracks and fissuring, which are typical of ductile striated growth
(c) Border between the light patch and the slow-growth area. The upper area shows a fan-shaped type of morphology, while the lower area is more amorphous and exhibits fissures perpendicular to the direction of growth

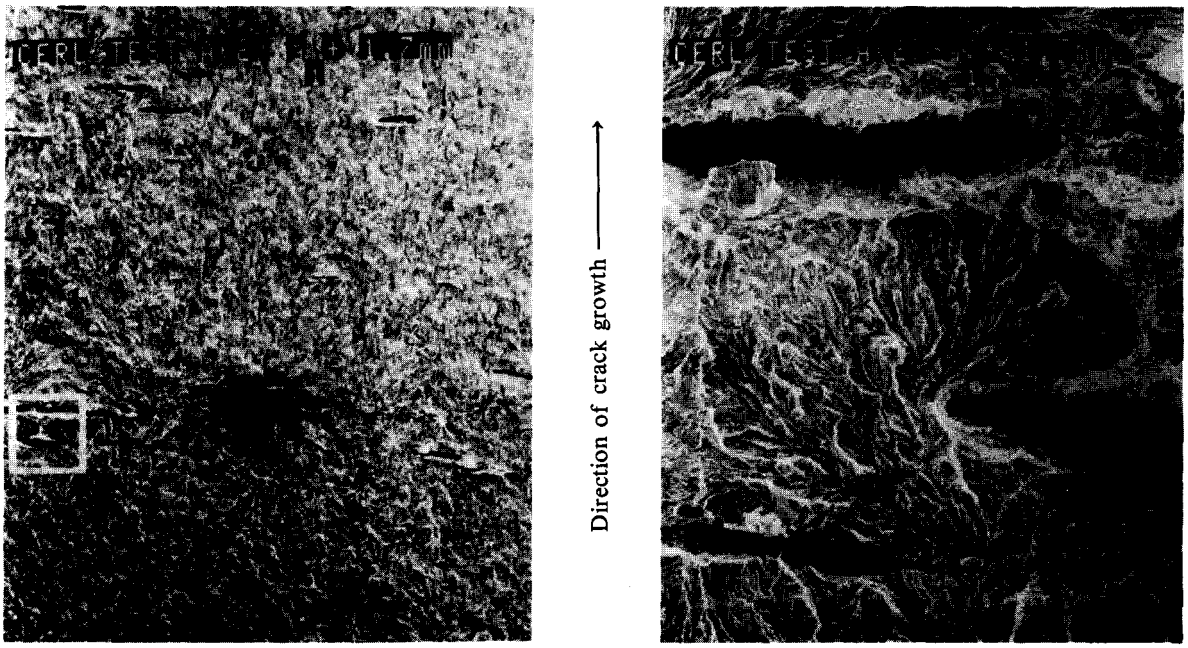

Fig. 17—Incidence and nature of elongated holes, $\Delta K \approx 26$ MPa $\sqrt{m}$
(a) General view, showing the elongated holes caused by inclusions
(b) Magnified view of the area boxed in (a), showing fan-shaped regions around the holes and individual inclusion sites within the elongated holes

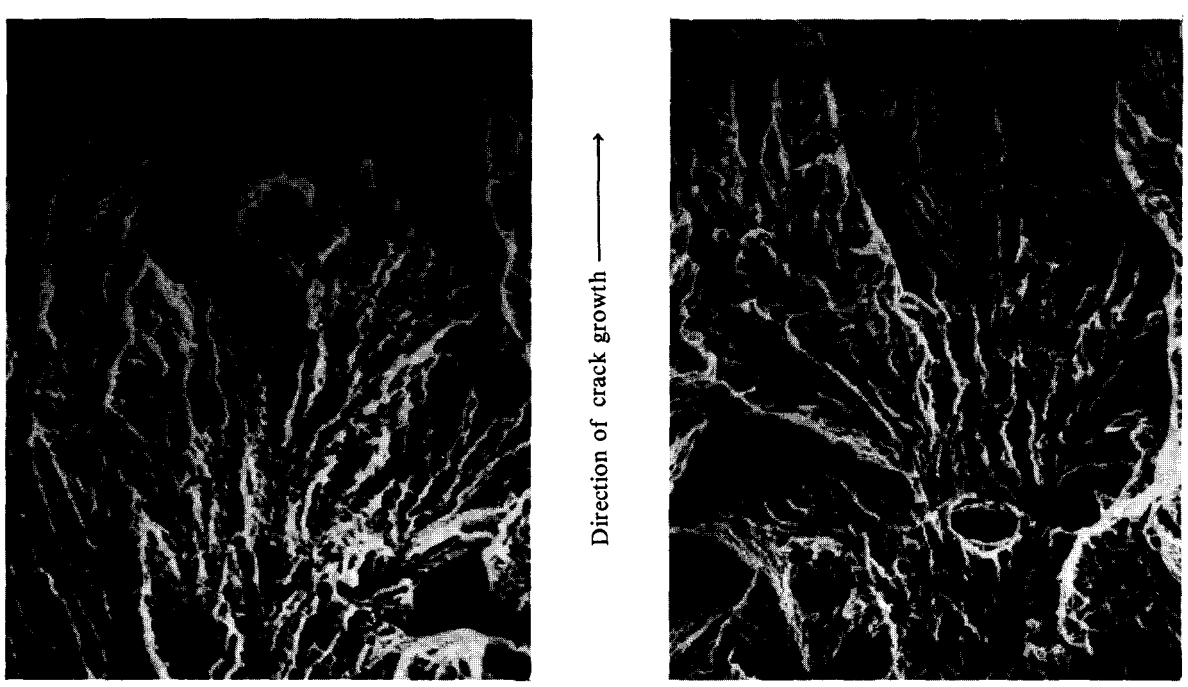

Fig. 18—Details of fan-shaped areas
(a) Evidence of striated growth within a fan-shaped area, $\Delta K = 29$ MPa $\sqrt{m}$, average spacing = $1{,}8 \times 10^{-}$ mm
(b) Fan-shaped area showing evidence of ductile ridges with little striated growth, $\Delta K = 28$ MPa $\sqrt{m}$

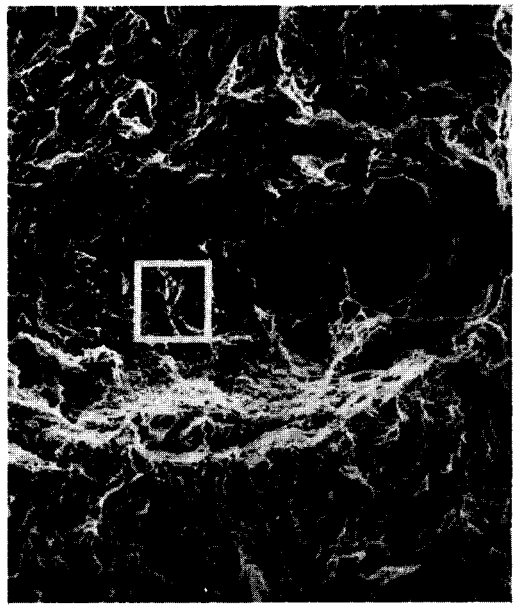

(a)

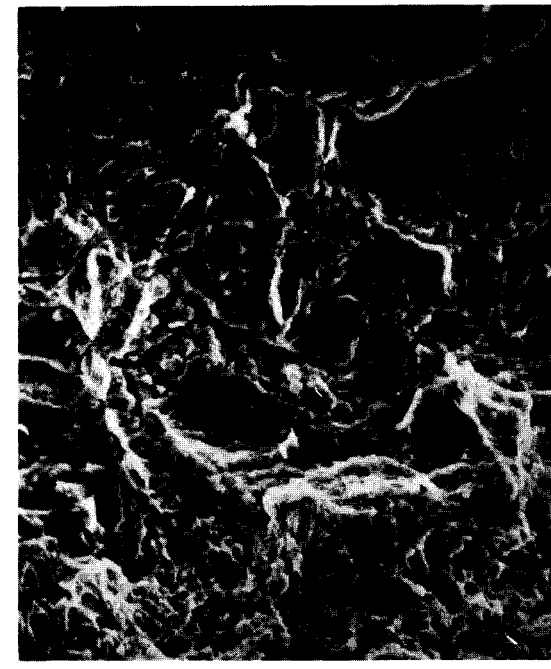

(b)

Fig. 19—Details of the flat amorphous areas associated with inclusion sites at plateau ΔK levels
(a) Flat, featureless region about 0,3 mm in size
(b) Magnified details of the boxed region in (a)

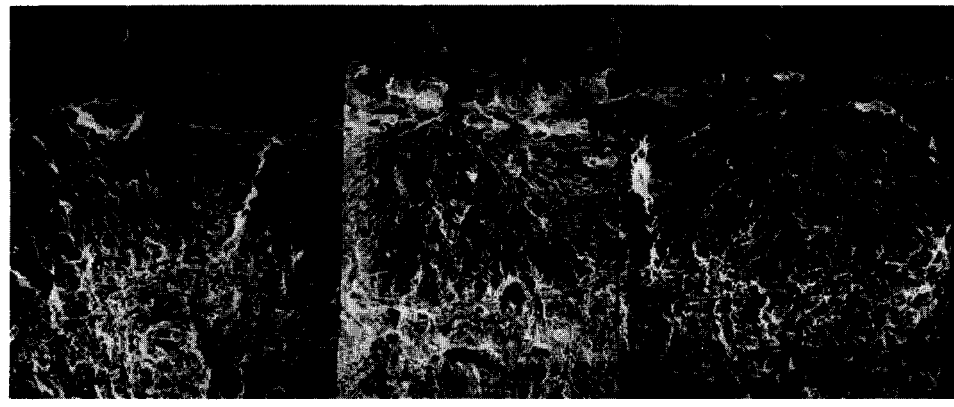

Fig. 20—Initial crack growth in test C*1. At the top of the photomicrographs is the air-precracked region. The initial growth is fan-shaped in character and starts from sites of non-metallic inclusions. The topography is much flatter at the bottom of the photomicrograph, with fissures perpendicular to the general direction of growth, which indicates transgranular ductile striated growth

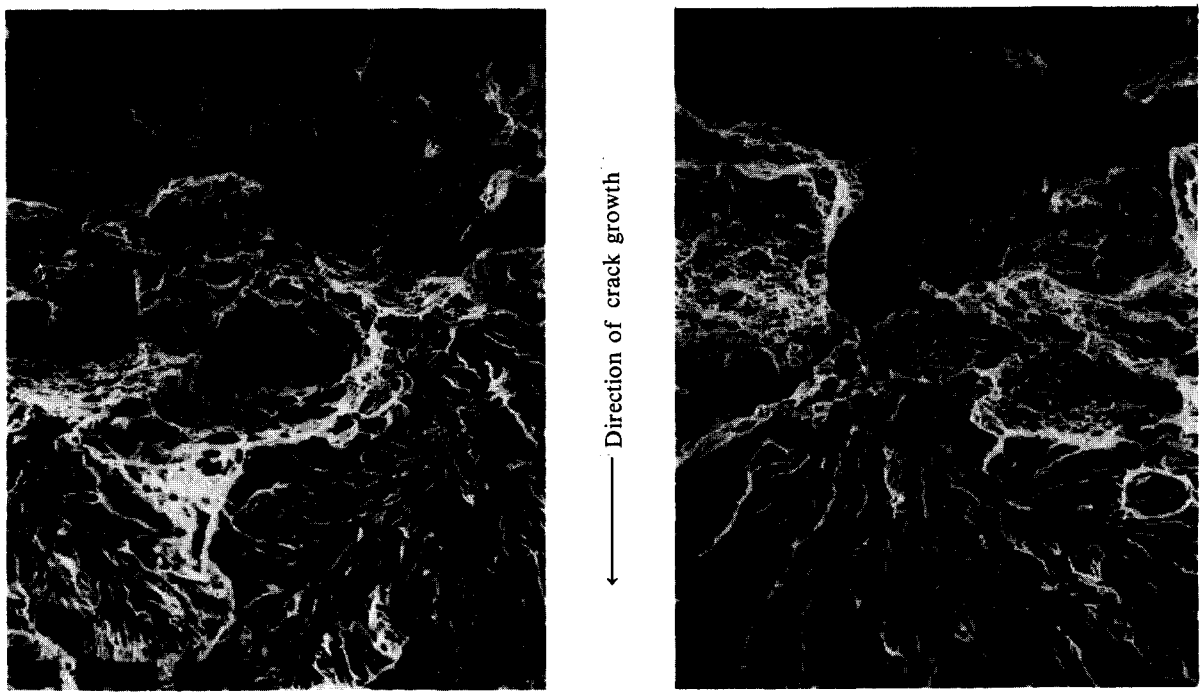

Fig. 21—The initiation of fan-shaped EAC growth associated with elongated clusters of non-metallic inclusions. Individual inclusions are about 20 μm in diameter

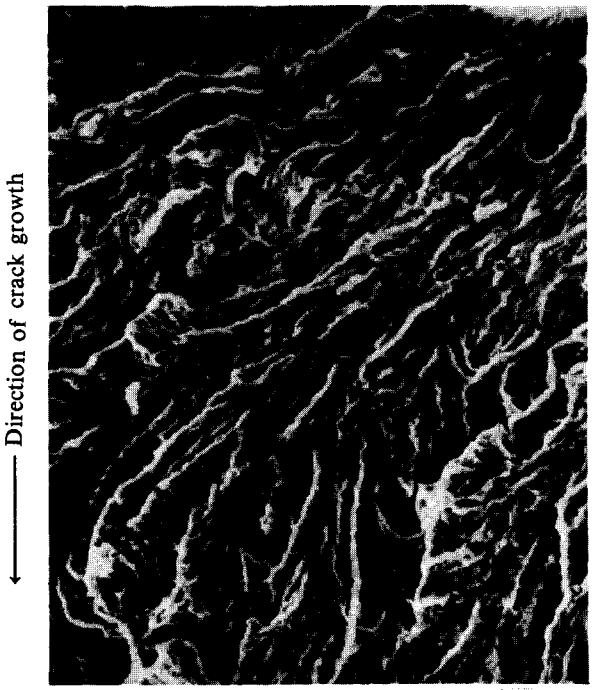

Fig. 22—Details of initial fan-shaped growth, with little evidence of striations

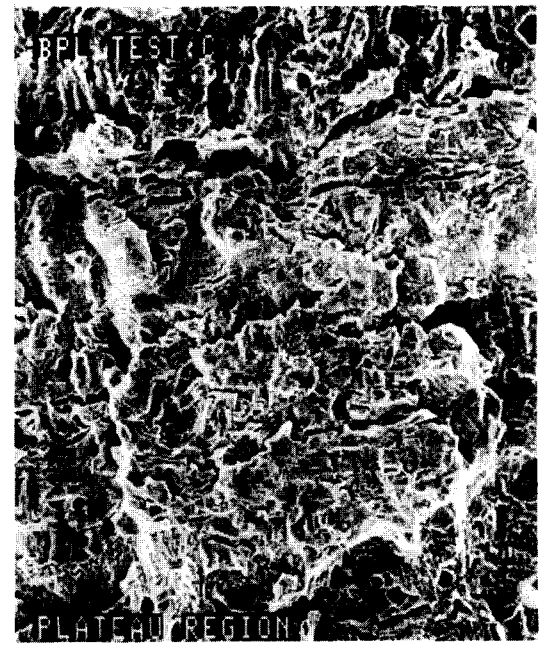

Fig. 23—Details of the type of growth during plateau formation, showing fissured features indicative of ductile striated growth

as the lower part shows fan-shaped growth, which was typical of the rosette, while the top shows fissured growth typical of transgranular ductile striated fatigue fracture. The latter fracture mode was prevalent in almost all the fatigue fracture surfaces in the macro fan-shaped region. The volcano-type initiation sites are further illustrated in Fig. 27, which shows evidence of ductile striated growth prior to the fan-shaped region (top of photomicrograph).

The area around these initiation sites was subjected to detailed examination, but few features of any note were found. However, because of the ridge-type appearance in this region, it was decided to view this region from the precracked region; this is shown in Fig. 28. Figure 28(a) illustrates that the initiation region is associated with a large step in the crack path, while Fig. 28(b), utilizing the tilt facility of the SEM, shows that the step is asso-

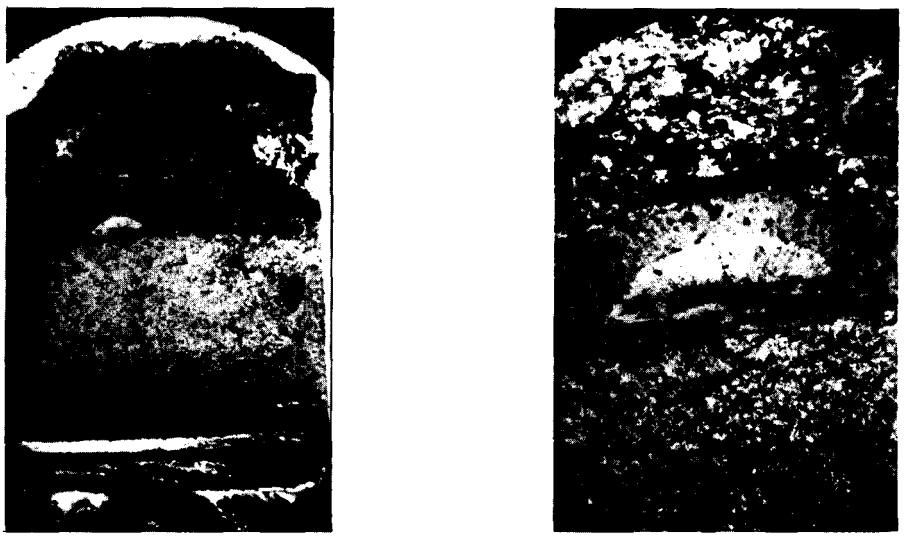

Fig. 24—Details of the rosette formation in test C*2
(a) Macro details of rosette formation (× 1,2)
(b) EAC rosette region initiated ahead of the precracked region

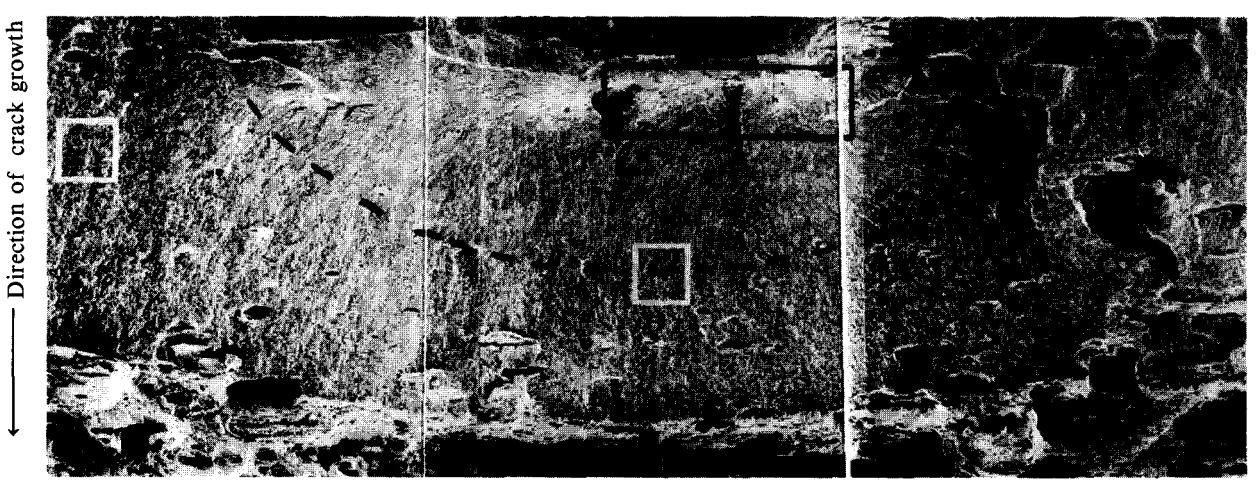

Fig. 25—Composite photomicrograph of the macro fan-shaped region (demarcated by the broken line) shown in Fig. 21. There is a sudden change in morphology at the boundary of the fan-shaped region. Also evident are the volcano-type features that are associated with the initiation site of the macro fan-shaped region

ciated with a massive inclusion site—about 1,3 mm in length. This area had contained type I and type II (rod-like) inclusions of manganese sulphide, which had dissolved during the tests. Another view of the initiation site of the rosette region is given in Fig. 29, which essentially gives a tilted view of the boxed region in Fig. 25; again, type I and II manganese sulphide inclusion sites are evident. The right side of this photomicrograph shows two interesting features: the fan-shaped growth that initiated from this region runs out in *all* directions, i.e. fan-shaped growth runs both along and against the general direction of growth (Fig. 30); and (b) there is a significant region of intergranular failure (Fig. 31) showing 'yawning' grain boundaries that have been substantially separated.

Test C*3 (Sinewave)

A section (Fig. 32) of the broken fracture surface from RR & A test C*2 was supplied to BPL for fractographic analysis.

Pre-threshold—Region I (ΔK < 21 MPa $\sqrt{m}$) Ductile Striated Crack Growth

In Fig. 32 the dark-coloured area is the region of air-crack growth and shows the beach marks associated with each increase in ΔK. The predominant failure mode in this region was ductile striations. An interesting macro feature in this dark-coloured region is the occurrence of elongated lighter regions, especially towards the left-hand side of the specimen, which are not unlike region II cracks.

Details of two of the isolated lighter regions are exhibited in Figs. 33 and 34. Fig. 33 shows a detailed composite picture of the light-coloured region, designated point A in Fig. 32 that occurred abruptly at the ΔK =

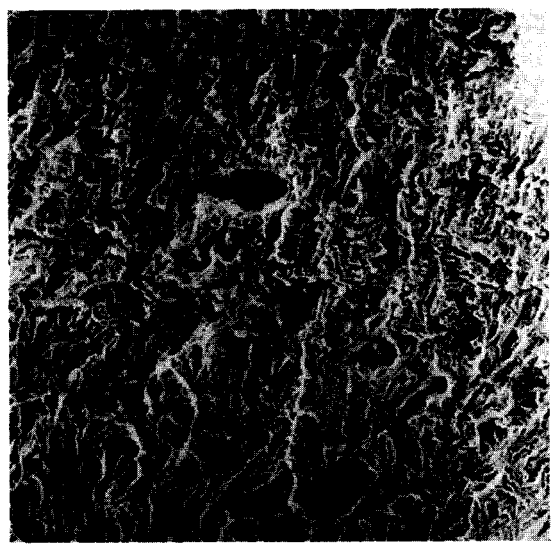

Fig. 26—Boundary region of a macro fan-shaped region, showing the abrupt change in fracture morphology: the lower region shows fan-shaped growth, while the upper shows fissured growth indicative of ductile striated growth

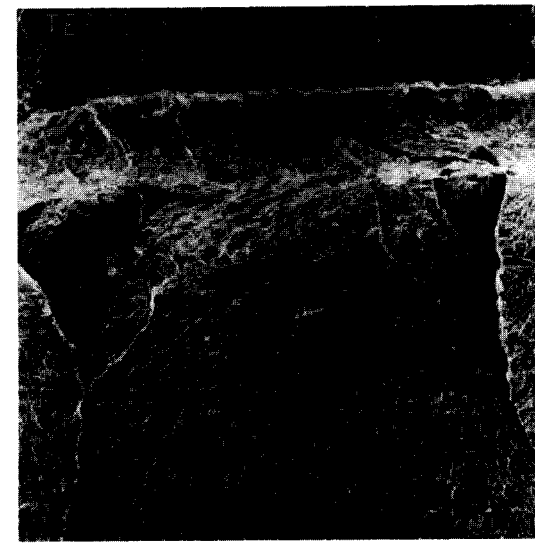

Fig. 27—A detailed view of the region associated with the initiation site of the macro fan-shaped area, showing volcano-type features associated with a large change in crack path and fissured striated growth prior to the initiation site (top of photomicrograph)

(a)

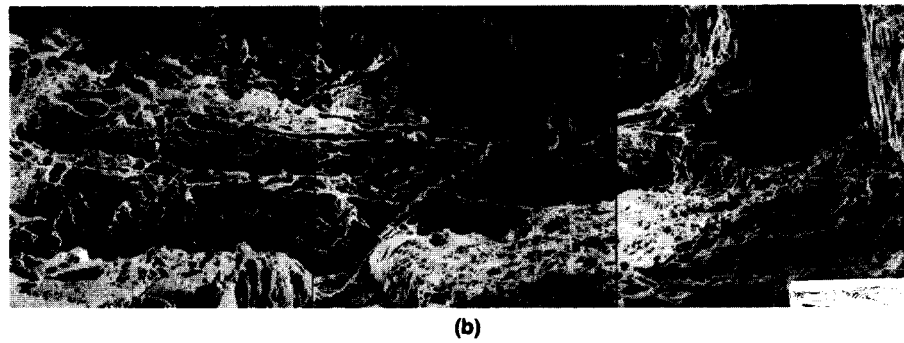

(b)

Fig. 28—Initiation region viewed from the precracked area
(a) View from the precracked region, showing the large step associated with the initiation sites of the macro fan-shaped region
(b) Tilted view of the stepped region associated with initiation sites, showing the massive inclusion site about 1,3 mm long where there is evidence of type I and type II (rod-like) manganese sulphide inclusions

II manganese sulphide inclusions. Features at the right-hand side of the photomicrograph show that fan-shaped regions run from the initiation site in *all* directions, and that there is a region of intergranular failure

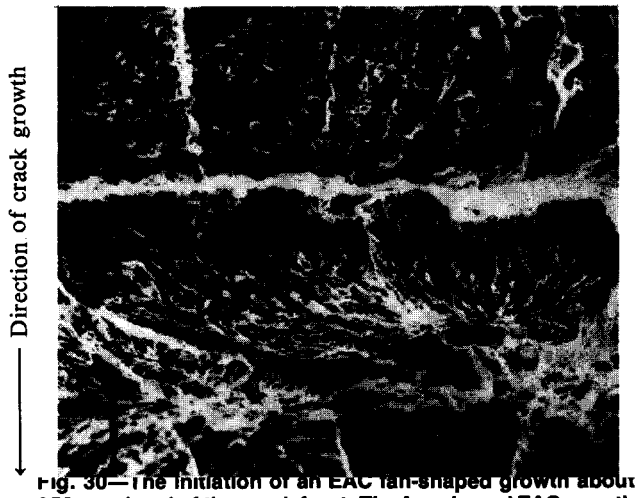

Fig. 30—The initiation of an EAC fan-shaped growth about 250 μm ahead of the crack front. The fan-shaped EAC growth in this case is in the direction opposite to the general direction of crack growth

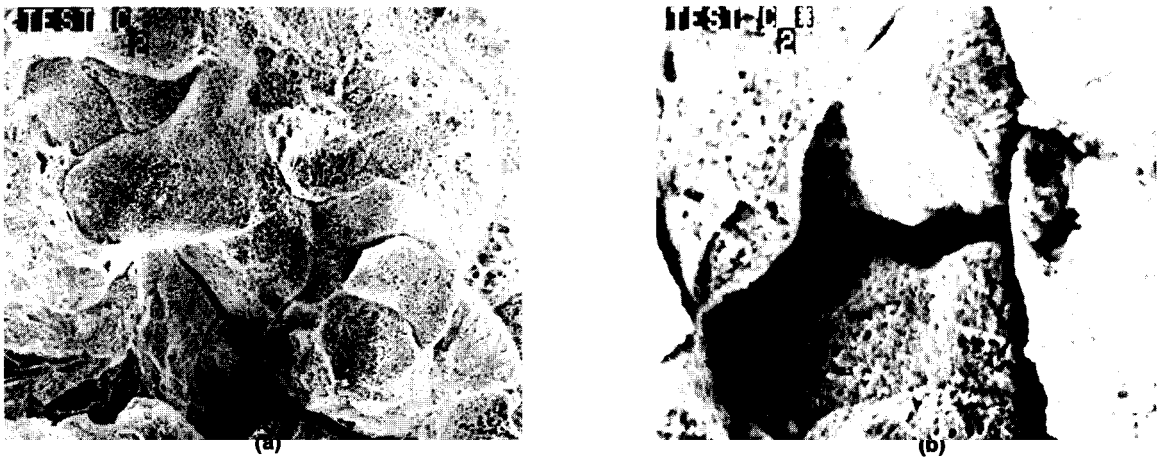

Fig. 31—Details of the region showing intergranular failure, the region being associated with the initiation site of the macro fan-shaped region

(a) General view (b) Detailed view, showing 'yawning' grain boundaries

18 MPa $\sqrt{m}$ step during testing. This photomicrograph shows the occurrence of fan-shaped growth between a small fissure running parallel to the direction of growth and step ΔK = 18 MPa $\sqrt{m}$. However, the fan-shaped growth was not sustained, but lasted only about 0,5 mm before the fracture mode abruptly changed to ductile striated growth (shown by the broken line in Fig. 33). This fan-shaped growth is similar to that found in numerous tests that exhibited region II EAC growth.

Fig. 34 shows another instance of a long finger of light-coloured region (as at point B, Fig. 32) surrounded by a darker-coloured EAC region (ductile striated region). Here, a thin ribbon (0,2 mm thick and 1,4 mm long) of fan-shaped growth runs out at right-angles from a large fissure and is surrounded by ductile striated growth; the boundary is shown by broken lines.

In both instances these light regions are, in fact, small localized bursts of EAC growth (region II), and are associated with fissures running parallel to the general direction of crack growth.

Another interesting instance of EAC growth is shown in detail in Fig. 35. The area between the ΔK steps 18 to 21 MPa $\sqrt{m}$ is shown in Fig. 35(a), from which it is evident that the ΔK = 21 MPa $\sqrt{m}$ beach mark exhibits a localized bowing out (of about 1 mm) in the vicinity of a fairly large fissure. This is the result of the sudden localized occurrence of fan-shaped EAC growth (broken lines) between the ΔK steps 18 to 21 MPa $\sqrt{m}$. Fig. 35(b) shows details of the edge of this EAC region, exhibiting a change from ductile striated growth to fan-shaped growth in Fig. 36(c), and the continuation of fan-shaped EAC growth beyond the beach mark ΔK = 21 MPa $\sqrt{m}$. The initiation for this region II growth was the front tip of the fissure running parallel to the direction of crack growth; this is illustrated in Fig. 36(b). A general low-magnification view of this is shown in Fig. 37.

As a result of the occurrence of a number of deep fissures running parallel to the direction of crack growth and their association with localized bursts of region II EAC growth, the exact nature of these fissures was investigated. By use of the tilt mechanism, it was possible to obtain some details of the sides of selected fissures; these are shown in Fig. 38.

Figs. 38(a) and (b) show that these fissures are associated with the occurrence of massive clusters of non-metallic inclusions, mainly type I and type II (rod-like) manganese sulphides. These findings are supported by the sulphur print, taken a few millimetres below the fracture surface (Fig. 39).

Regions II and III (ΔK > 21 MPa $\sqrt{m}$) EAC Growth

When the ΔK level increased to 21 MPa $\sqrt{m}$, the total thickness of the test sample exhibited fan-shaped EAC growth (light region in Fig. 32, and also Fig. 40), and the growth rates increased dramatically. Within the rapid growth region, the predominant fracture feature was a fan-shaped type of growth.

Immediately prior to the unstable post-test fracture, the main fatigue-crack front is very uneven and exhibits two instances (Fig. 32) of cracking that extended well ahead of the main crack front. Both are associated with deep fissures running parallel to the general direction of crack growth. Such an instance is shown in Fig. 41 and corresponds to box D in Figure 32. This photomicrograph shows the existence of a long ribbon (about 7 mm in length) running adjacent to a deep fissure that extends well into the unstable post-test region. No distinct boundary between this ribbon and the EAC growth region below ΔK = 25 MPa $\sqrt{m}$ was evident, and failure in this region was by fan-shaped growth identical to that in the EAC growth region (Fig. 42). Fig. 41 also shows the existence of terraced clusters of inclusions along the edge of the fissure at face D, and details of this face are shown in Fig. 43. The massive inclusion clusters comprise spherical type I and rod-like type II manganese sulphide inclusions.

DISCUSSION

Fractography

The observations recorded above on the test A4 and test C*3 specimens showed that isolated bursts of region II EAC growth can occur at ΔK levels below that for general region II growth, and can exhibit fan-shaped growth behaviour. Such isolated fan-shaped regions are invariably associated with large clusters of type I and type II manganese sulphide inclusions, which dissolved during the tests. These sudden 'pre-threshold' ΔK EAC growth transients are probably the result of the attainment of the right local chemistry at the tip of the crack, possibly through the dissolution of closely spaced clusters of manganese sulphide inclusions.

The abrupt cessation of these EAC growth areas may be the result of

(a) the washing out of the aggressive species at the tip of the crack,
(b) the non-attainment of some critical mechanical conditions, and
(c) the diffusion of positive hydrogen ions, H^+, away from the tip of the crack.

Thus, there may be a need for some complex critical balance to be attained between the chemistry at the tip of the crack and imposed mechanical conditions before total EAC growth occurs, with a concomitant fast growth of fatigue cracks.

One interesting feature is the occurrence of a region of EAC growth within the ΔK steps 18 to 21 MPa $\sqrt{m}$ (Fig. 37). A schematic diagram of growth events is given in Fig. 44, showing that, if there had been a regular crack front during the ductile striated growth (broken line), the crack in the region of the fissure would have grown a further 0,14 mm if EAC had not occurred. Thus, according to the growth rates in Test C*2, at ΔK = 20 MPa $\sqrt{m}$, da/dN would be about 1×10^{-4} mm per cycle for non-EAC growth. This means essentially that the EAC growth facet, 1,45 mm long, was formed in 1400 cycles, yielding a rate for EAC growth of $1{,}1 \times 10^{-3}$ mm per cycle. This value approaches the plateau rates where general EAC growth occurred across the total width of a specimen.

In test C*1, there was an example of region II EAC growth that occurred across the total width of the specimen at the start of the test. The average length of this region is about 0,5 mm, and the incidence of clusters of non-metallic inclusions at the initiation sites of discrete fan-shaped facets is very high. This can be explained as follows.

Fig. 32—Details of the broken fracture surface from RR & A test C*. The largest boxed area represents the portion that was submitted to SEM examination

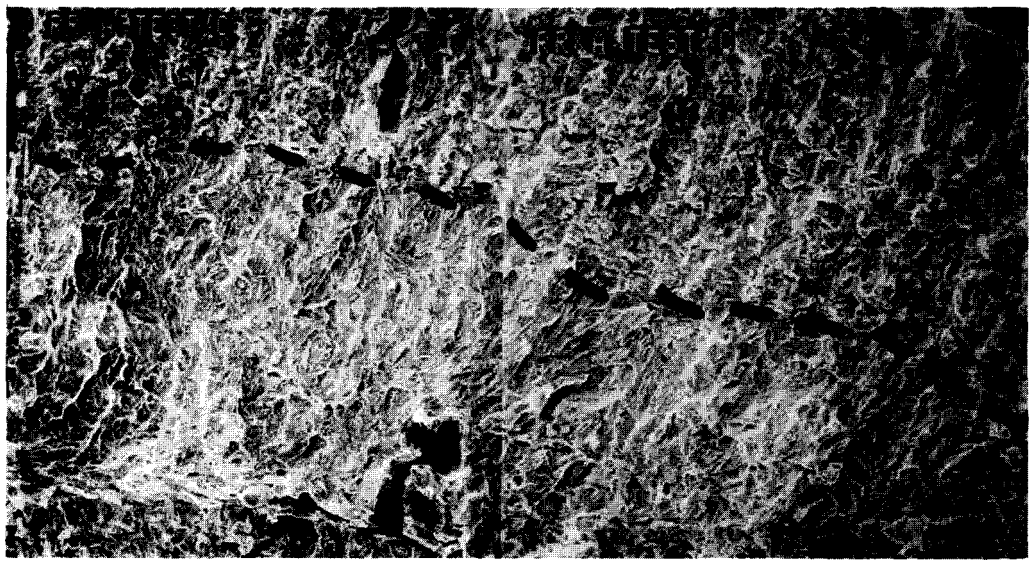

Fig. 33—A ribbon of the EAC region. This burst of fan-shaped EAC growth resulted from the increase in ΔK to 18 MPa $\sqrt{m}$, which is evident at the bottom of the photomicrographs. Again, this ribbon emanates from a large elongated cluster of inclusions (point A, Fig. 32)

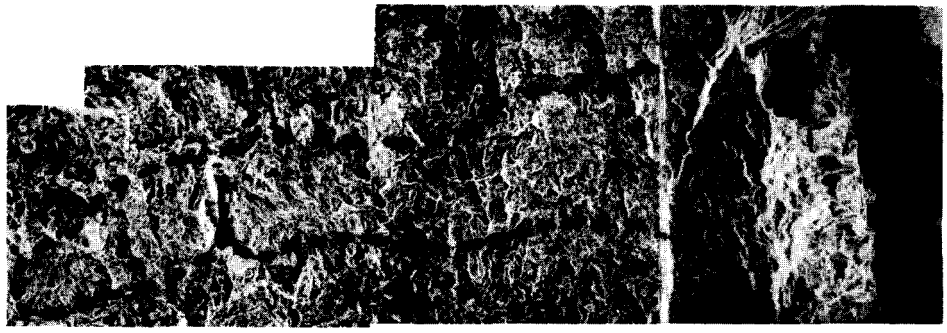

Fig. 34—A thin, long ribbon of light-coloured EAC region running perpendicular to the general direction of crack growth between ΔK = 18 and ΔK = 21 MPa $\sqrt{m}$ (point B, Fig. 32). This ribbon is about 1,4 mm in length and 200 μm thick, and is associated with a large elongated cluster of inclusions running parallel to the crack growth

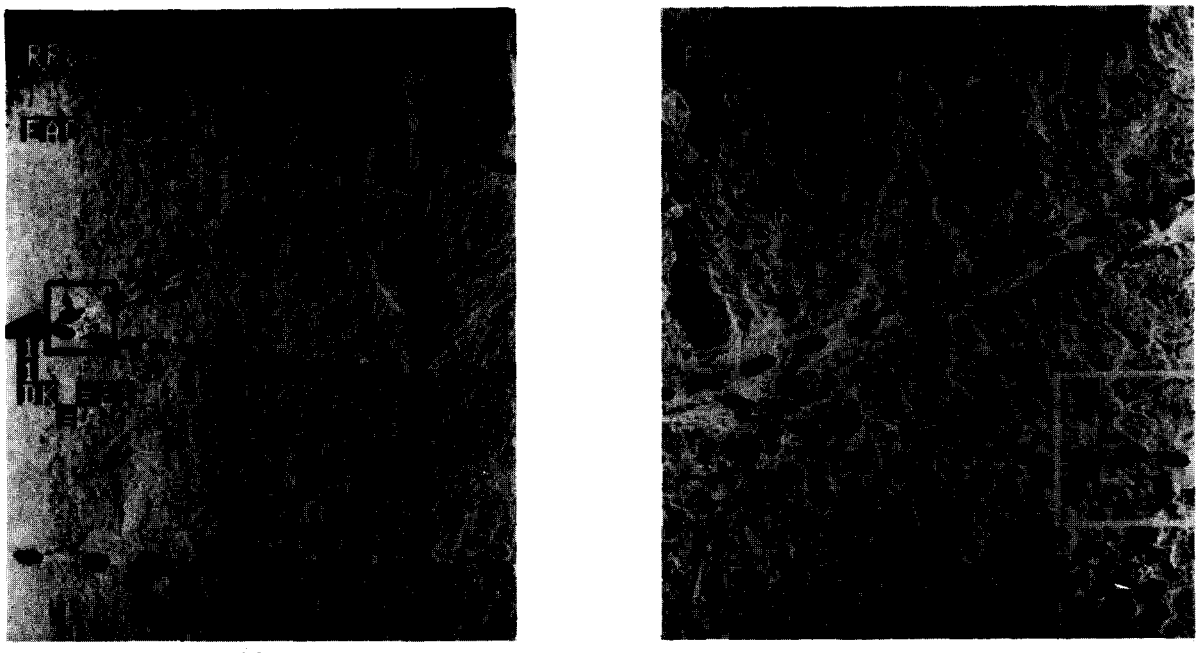

(a) (b)

Fig. 35—(a) General view of EAC region within the broken lines
(b) Details of boxed area in (a). The top part is the EAC region associated with step ΔK = 21 MPa $\sqrt{m}$. The middle, triangular region is EAC between the onset of fan-shaped growth and the step ΔK = 21 MPa $\sqrt{m}$. The bottom shows ductile striated growth associated with the step ΔK = 18 MPa $\sqrt{m}$

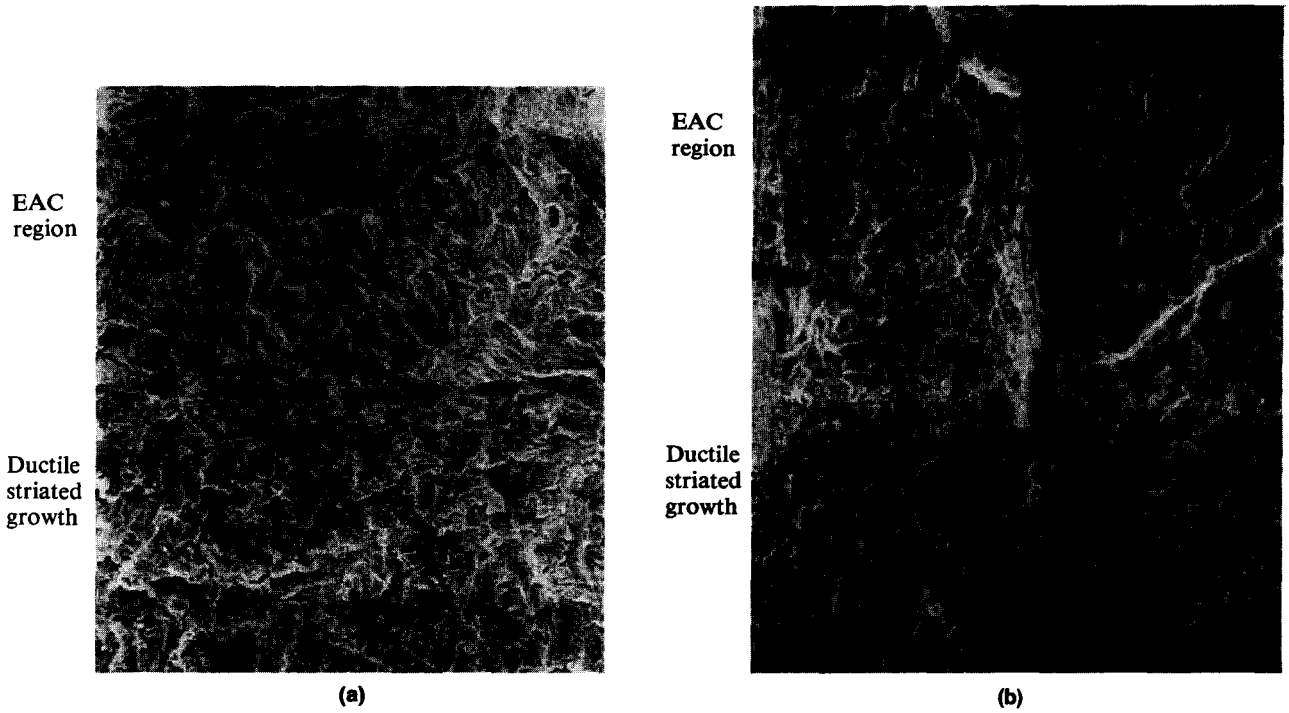

(a) (b)

Fig. 36—(a) Details of the boxed region in Fig. 35(b), showing the abrupt change to EAC growth within the step ΔK = 18 MPa $\sqrt{m}$
(b) Initiation site for the EAC region at the base of an elongated cluster of inclusions running parallel to the direction of crack growth

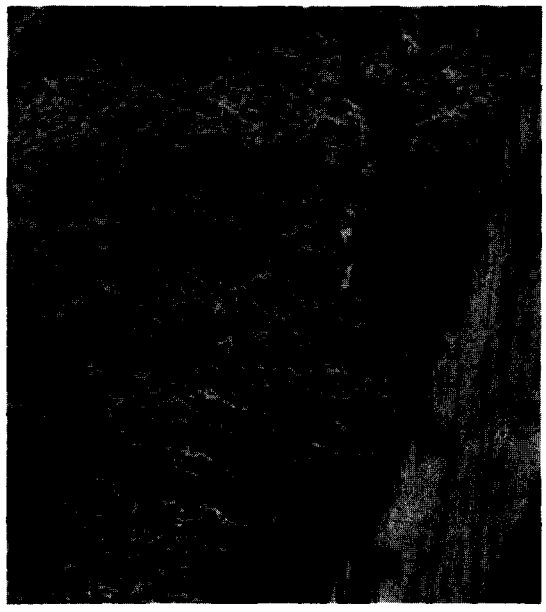

Fig. 37—Tilted view of EAC growth region at the step ΔK = 21 MPa $\sqrt{m}$

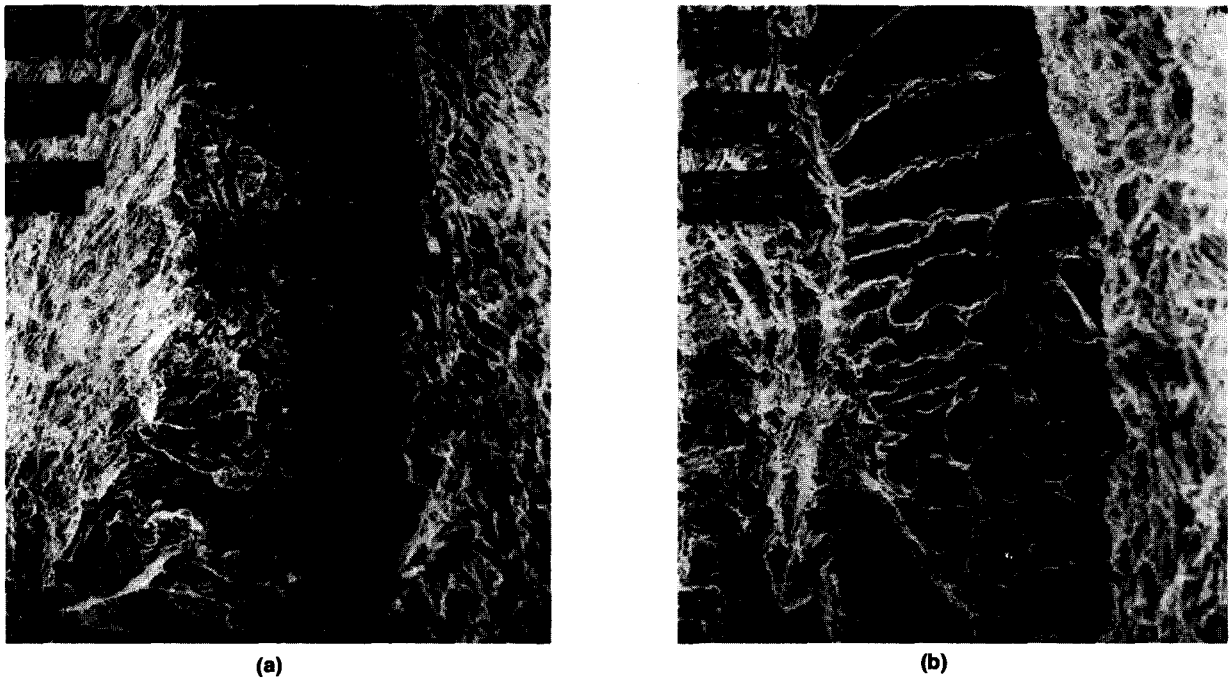

(a) (b)

Fig. 38—Details of elongated fissures, showing the sides associated with type I and II manganese sulphide inclusions (45° tilt)

Fig. 39—Sulphur print of face 2 mm from the fracture face, showing elongated clusters of sulphide inclusions (× 1)

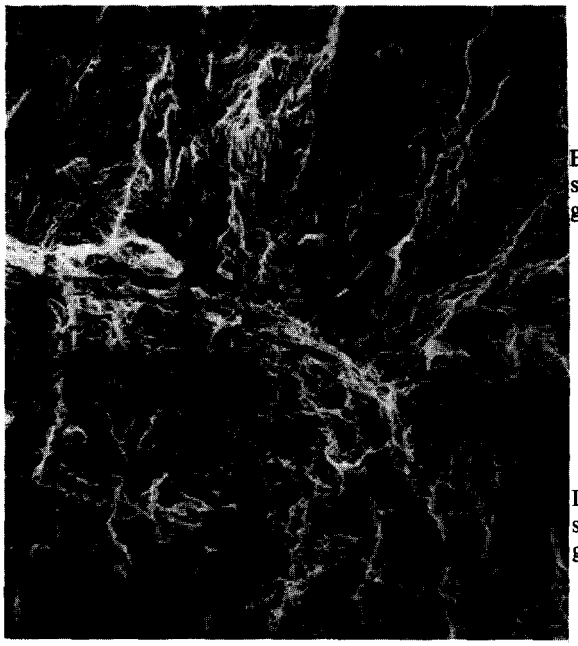

Fig. 40—Abrupt change in fracture characteristics from ductile striated growth to the fan-shaped growth indicative of EAC at the step ΔK = 21 MPa $\sqrt{m}$

Fig. 42—Details of the box D in Fig. 32, showing fan-shaped growth extending some 7 mm into the unstable post-fatigue region. Such growth is identical to the EAC growth found at ΔK < 25 MPa $\sqrt{m}$

Fig. 41—Region of unstable fracture beyond EAC region, i.e. ΔK > 25 MPa $\sqrt{m}$. A ribbon of fan-shaped growth about 7 mm long runs along the right-hand edge of the deep fissure (box D in Fig. 32). Evident are the terraced sides of the inclusion down face D

Fig. 43—Details of face D in Fig. 32 showing the massive inclusion clusters of types I and II manganese sulphide running along the edge of the fissure associated with the region of extended EAC growth

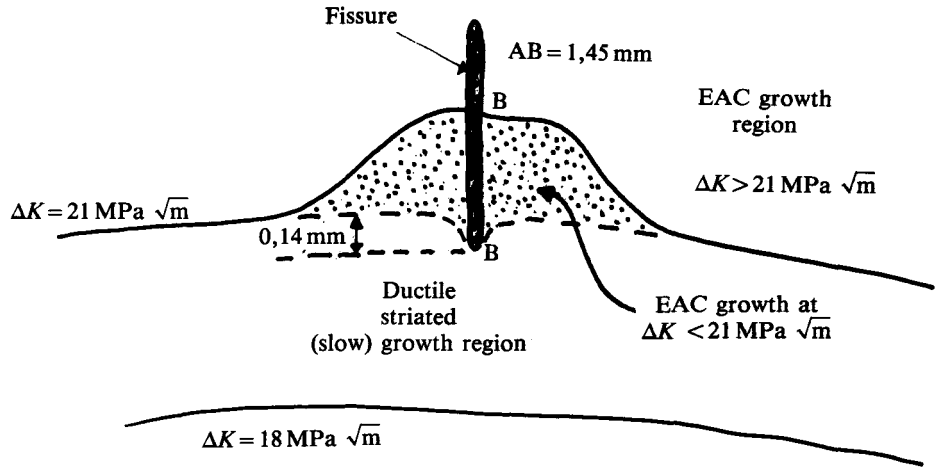

Fig. 44—Schematic diagram of the deviation in the step ΔK = 21 MPa $\sqrt{m}$ as a result of a semi-circular region of EAC growth within the ΔK range 18 > ΔK > 21 MPa $\sqrt{m}$. Approximate measurements were taken from Fig. 36. The growth rate in the slow-growth region was about 1 × 10^{-4} mm per cycle

Before the test started, the previous K_{max} at the tip of the crack was 30 MPa $\sqrt{m}$, which increased to 107 MPa $\sqrt{m}$ (ΔK = 15 MPa $\sqrt{m}$) during the test sequence. This represents a change in the size of the plain-strain plastic zone from 0,4 to 5 mm. Since sulphide inclusions within this plastic zone undergo decohesion, with the matrix at stresses near yield level, this large increase in the size of the plastic zone will easily seek out inclusion clusters immediately beyond the tip of the crack. It is envisaged that these easy fracture paths along the length of the tip expose numerous inclusion sites; the aqueous environment then dissolves these inclusions, thus forming a more acidic environment that favours the growth of environmentally assisted fatigue cracks by a possible mechanism of hydrogen embrittlement.

Exactly why the fan-shaped growth stops so abruptly after 0,3 to 0,8 mm of growth is not easily explained, but it could be due to a lack of the 'right' inclusions around the tip of the crack. Thus, the aggressive crack-tip environment would not be sustained, and ductile striated growth could ensue.

The above results may explain the order-of-magnitude difference between the plateau growth rates attained in test C*3 and those in test C*1. It is possible that, in test C*3, fan-shaped growth was sustained for a longer period, thus enabling high rates of plateau growth to be reached. It is also possible that the difference in initial crack lengths in this test (15 mm in Test C*3 as against 30 mm in Test C*1) corresponded to markedly different inclusion densities and/or orientation effects.

Indeed, Test C*3 was conducted on BSC A533B plate in the T-L orientation, and the elongated inclusion clusters therefore ran parallel to the direction of crack growth (Fig. 32) while, in the Marrel Frere A533B plate (0,006 % S), the inclusion clusters ran perpendicular to the general direction of crack growth (Fig. 11). Thus, a crack growing through this material would sample more inclusion clusters for a longer time period.

The average length of the initial EAC growth ribbon in test C*1 was about 0,5 mm. A plot of crack length versus number of cycles is shown in Fig. 45. It is evident that this average distance agrees remarkably well with the limited region II EAC growth.

The results of test C*2 show the existence of a large rosette of region II EAC growth. Outside this feature, the fracture mode was totally of the ductile striated type characterized by fissures at right-angles to the general direction of crack growth. Furthermore, the region at which the macro fan-shaped region initiated has been shown to consist of an elongated cluster of non-metallic inclusions, consisting mainly of type I and type II manganese sulphides that dissolved during testing in a PWR environment. Also evident near the initiation region were areas of intergranular failure with 'yawning' grain boundaries typical of hydrogen-assisted cracking. Fractographic evidence (Fig. 30) shows that fan-shaped growth is initiated ahead of the main crack front and then fans back in the opposite direction to general crack growth, this again pointing to a hydrogen-assisted mechanism. The graph of the length of the raw crack versus the number of cycles in test C*2 is given in Fig. 46. The curve shows a definite deviation at $a/w \simeq 0{,}615$: initially, crack growth typically increased with crack length but, at $a/w \simeq 0{,}615$ the growth rate abruptly slowed down to the initial rates and then increased again with crack length. Also shown on this graph is the range of crack lengths over which the rosette region developed. The region of fastest growth agrees well with the initial development of the rosette, while the point of abrupt change in crack growth coincided with the outer boundary of the fan-shaped region. Thus, although the macro fan-shaped region of EAC represents only about 17 per cent of the specimen thickness, it appears that the crack-monitoring instruments sensed its development during the test.

In addition, two interesting features were observed in test C*2: (i) the initiation site for rosette formation was approximately 0,3 mm ahead of the main crack front, and (ii) intergranular failure at the initiation site exhibited grain-boundary 'yawning' that is typical of a hydrogen-embrittlement mechanism.

Manganese Sulphide Inclusions

The solid solubility of sulphur in iron is very low, and for the present discussion all the sulphur present in steel

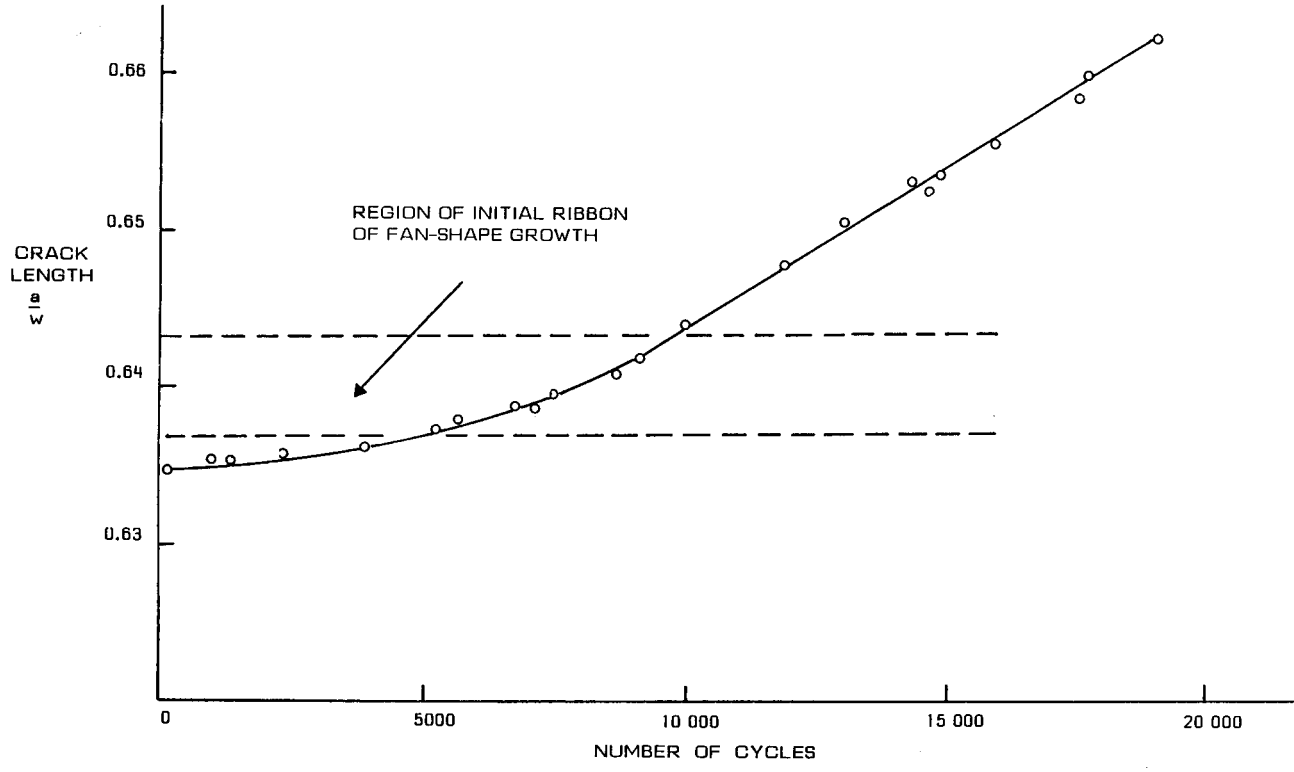

Fig. 45—The length of a raw crack versus the number of cycles in BPL test C*1, showing that the initial formation of a ribbon of fan-shaped EAC growth coincides with the fastest recorded growth rate

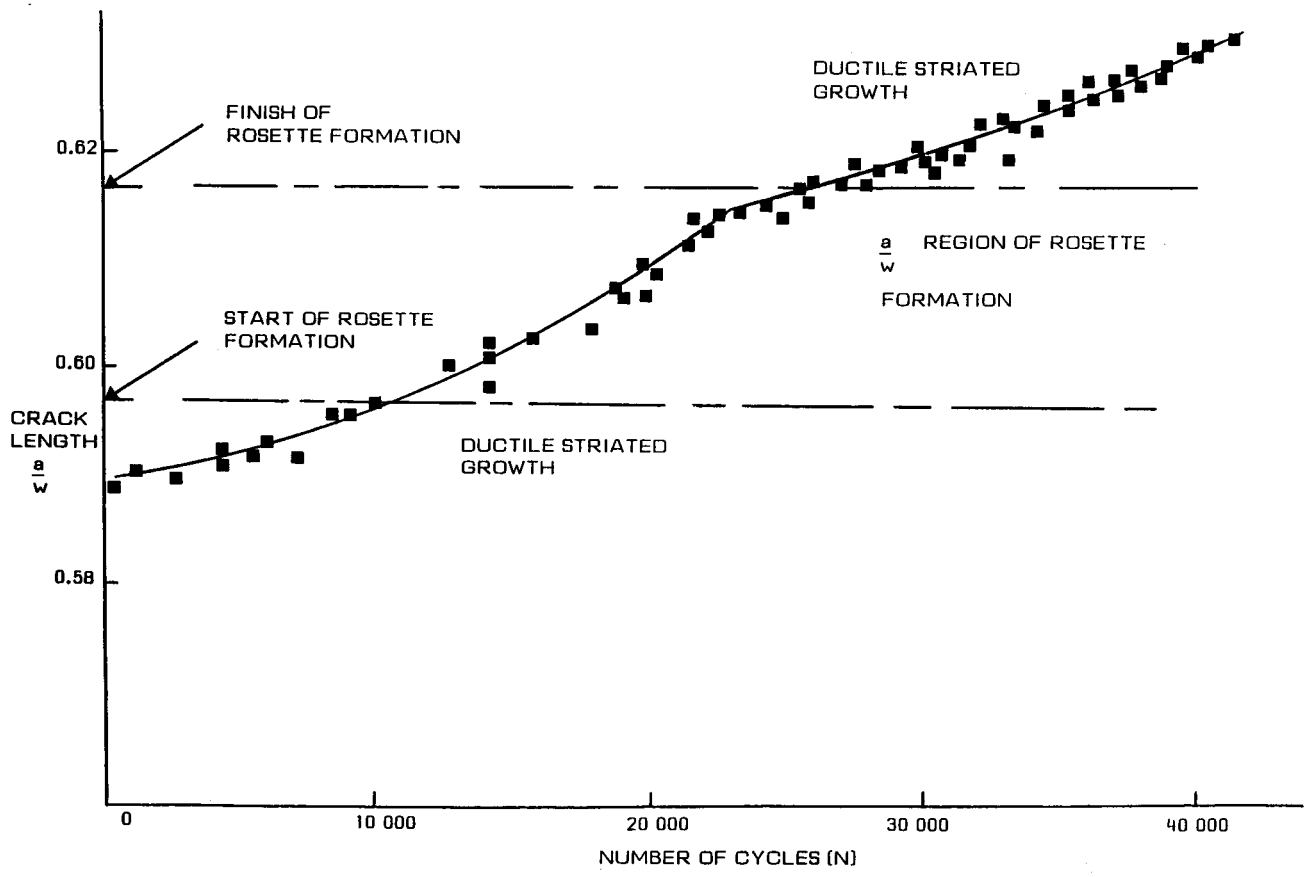

Fig. 46—The length of a new crack versus the number of cycles in BPL test C*2, showing the region of rosette formation

can be regarded as being precipitated as a sulphide phase (mainly manganese sulphide). One can easily calculate the number and inclusion spacing by assuming that all the sulphur exists as equally sized spherical manganese sulphide inclusions and knowing the bulk sulphur level; for example, by assuming 10 μm for a steel containing 0,001 per cent sulphur. However, it has been shown that the cleanliness expressed by a bulk sulphur level is in itself inadequate to characterize a steel. The influence on the steel properties of similar bulk sulphur levels can vary widely, depending on the size and distribution of the sulphide inclusions. Therefore, parameters other than sulphur content must be considered.

The volume fraction of manganese sulphide inclusions can be calculated by the equation[4]

(Vol. fraction MnS) V_{MnS} = 0,053 (% S).

Thus, for a sulphur level of 0,006 per cent (V_{MnS} = 0,032%), the inclusion sites observed on numerous fatigue fracture surfaces show varying inclusion diameters of 10 to 50 μm, giving a range of calculated spacings of 70 to 140 μm. However, fracture surface observations (Figs. 10, 11, 13, and 44) show the existence of elongated clusters of manganese sulphide inclusions, exhibiting localized spacing values of only a few micrometres running perpendicular to the general direction of crack growth. Thus, in the steel containing 0,006 per cent sulphur, grossly segregated regions, sometimes over 1 mm in length, that have V_{MnS} values in excess of 1000 times the value expected under ideal conditions, are a fairly common occurrence. Also, as a result of such segregated regions, there was little evidence of isolated manganese sulphide inclusions on the fracture surface, and the average spacing of the inclusions (in this case, the clusters of inclusions) was 300 to 700 μm, i.e. much longer than the idealized calculated values of 70 to 140 μm.

Torronen *et al.*[5] recently reported a link between EAC growth and manganese sulphide inclusions and showed that, if the size of the monotonic plastic zone in the growth direction exceeds the average inclusion spacing, EAC growth is sustained, i.e. the dissolution of one inclusion every 300 μm is sufficient to promote and sustain a localized hydrogen-induced cracking mechanism.

By use of the equations

R_M (size of monotonic plastic zone) = 0,036 $(K_{max}/\sigma y)^2$ (m) and

R_R (size of reversed plastic zone) = 0,106 $(\Delta K/2\ \sigma y)^2$ (m),

the following values were obtained for the onset of EAC growth:

Test A1 R_M = 2,3 mm, R_R = 150 μm

Test A2 R_M = 2,4 mm, R_R = 150 μm

Test A3 Isolated EAC growth R_M = 2,8 mm, R_R = 180 μm

*Test C*1* R_M = 3,6 mm, R_R = 60 μm

Continuous fans average 0,5 mm in length, i.e. 0,14 of R_M and 8 times R_R.

*Test C*2* R_M = 4,6 mm, R_R = 60 μm

Isolated rosette = 1,7 mm (max.), i.e. 0,48 R_M and 28 times R_R.

EAC initiated 0,3 mm ahead of main crack, i.e. 0,08 of R_M and 5 times R_R.

From these calculations, it can be seen that, where the EAC growth is isolated (tests C*1 and C*2), the extent is less than the size of the monotonic plastic zone and several times the size of the reversed cyclic plastic zone, i.e. there is no clear relationship between the two values of plastic zone and the size of the EAC region.

Finally, it is pertinent to mention the results generated by the BPL waveform programme[2]. Sine and triangle waveform tests were carried out under different mechanical test conditions, and in three instances the triangle waveform specimens did not show EAC growth, while the sine waveform specimens exhibited plateau-type EAC growth. In one test, however, EAC growth behaviour was exhibited in the specimens of both types of waveform; this apparently anomalous result can be explained if we consider the sulphur segregation pattern of the test specimen (Fig. 47). This figure shows that the initial crack front coincides with an elongated cluster of manganese sulphide inclusions; thus, the local chemical conditions at the crack tips may be right for the general onset of fan-shaped EAC growth regardless of the imposed mechanical waveform. This critical nature of the local distribution of the inclusions triggering and/or sustaining EAC growth was also shown in test A3, where isolated EAC growth occurred in two instances. Thus, although waveform plays some role in EAC growth, its effect is swamped by localized segregation of the inclusions, i.e. if the local chemistry at the crack tips is favourable, EAC growth occurs irrespective of the imposed waveform.

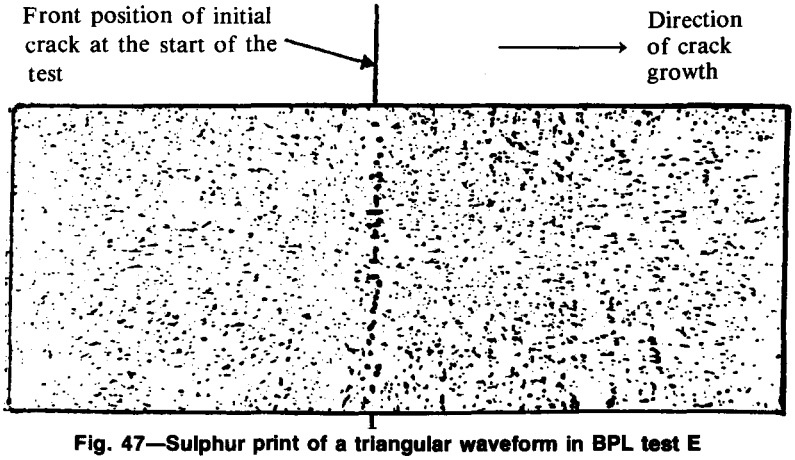

Fig. 47—Sulphur print of a triangular waveform in BPL test E

SUMMARY AND CONCLUSIONS

Fractographic studies on various specimens from high-R corrosion-fatigue tests have shown that the incidence and distribution of non-metallic inclusions (manganese sulphides) strongly affect EAC growth. Some features suggest that a hydrogen-assisted mechanism is responsible for EAC effects. The incidences of transient EAC growth in isolated regions suggest that the critical condition to trigger this type of growth represents the attainment of the 'right' local chemistry at the crack tips and favourable mechanical conditions.

ACKNOWLEDGEMENTS

The author gratefully acknowledges the financial support given to this work by the Central Electricity Generating Board. He is also grateful for the many invigorating discussions held with Dr J.D. Atkinson (CERL), and for the co-operation of D. Swan (RR & A).

REFERENCES

1. TOMKINS, B. U.K.A.E.A. *Report* ND-R-842(S), HMSO, 1982.
2. BULLOCH, J.H. *Res Mechanica,* vol. 18. 1986. p. 331.
3. BAMFORD, W.H. *Trans ASME, J.* Pressure vessel, Tech. 102. 1980. p. 433.
4. SPEICH, G.R., and SPITZIG, W.A. *Metall Trans.*, vol. 13A. 1982. p. 2230.
5. TORRONEN, K. *et al.* Fracture and role of microstructure. vol. 2, *Fatigue* 1983, EMAS, UK. p. 539.

Computerized data logging

A computerized data-logging system at JCI's Doornkop Gold Mine takes metal-accounting procedures through a quantum leap across out-of-date manual calculations into real time, where decisions can be based on minutes-old information. Metal accounting is used to determine how well a mine is doing. Key calculations involve the quantity of gold recovered as a ratio of ore crushed.

The manual system traditionally used is somewhat irksome, involving voluminous ledgers, which are painstakingly written up by metal-accounting clerks. Assay results from various points in the plant give an indication of the recovery rate, but the manual calculations involved are time-intensive and the results are often several days in arrears.

When JCI's Randfontein Estates Gold Mining Company commissioned its Doornkop Plant in the second half of 1984, the Consulting Metallurgist and other senior engineers were determined that a more efficient system should be installed.

A Process Controller had been ordered from Delta Controls (ALTEC) to measure flow and throughput via associated instruments, etc. This was regarded as a special-purpose computer and it functions well, having been designed for operator control. Additional hardware and software for metal accounting would have added greatly to the cost of the operation, possibly some R200 000, and the engineers therefore started looking for an alternative system.

Lindsay Data Systems was approached through Delta Controls, and a feasibility study by Lindsay Software led to the conclusion that the main computer could be profitably accessed via a gateway, using the standard instrumentation BUS—in this case the HPIB BUS.

A standalone Hewlett Packard scientific desktop computer was connected on the HPIB BUS, and by this means the Process Controller could be interrogated every 8 hours for values at all the important process points on the plant. This system, together with manual input of assay and laboratory results, provides a continuous picture of the way the plant is performing in strict accounting terms.

One of the most remarkable aspects of the investigation was that very clear specifications were provided by Doornkop's Metallurgical Superintendent and his staff because they had been able to work on a Visicalc model of the required database involving all the different reports that would be needed. The requirements were presented in the form of a massive spreadsheet altogether dramatically different from the vague specifications software developers often receive from end-users. This led to completion in a relatively short time.

The documentation proved to be good enough to give a clear picture of the communications protocol that would be required, and it was therefore possible to write it blind ahead of time and, when the gateway arrived, the system was plugged in and it worked. From the startup, a continuous picture of the performance of the plant was available.

The value to the Randfontein Estates Gold Mines is that automatic data logging is provided at the end of each shift, and the metallurgists know that the data are correct. Human error has been reduced to a minimum, data entry problems have been overcome, and delays in getting data in are something of the past.

Data obtained from the system, combined with laboratory assays from different sampling points, are used to produce accounting reports, and an acceptable band of values has been established for each of the crucial processes in the plant. These bands of values are checked every 8 hours, enabling the metallurgists to spot faults long before they develop into problems.

A database of results obtained in the 90 preceding shifts enables the operators to make comparisons in real time by matching current results with historical patterns. It wouild be very time-consuming to calculate a 90-shift moving average by manual methods.

The system is clearly performing well in the gold-recovery process, but it can be adapted to perform equally well in the monitoring of process control in a variety of plants where data are available for sampling on an online basis.